NASA TECHNICAL MEMORANDUM

NASA TM X-72632

COPY NO.

NASA TM X-72632

NORMAL INJECTION OF HELIUM FROM SWEPT STRUTS INTO DUCTED SUPERSONIC FLOW

By Charles R. McClinton and Marvin G. Torrence

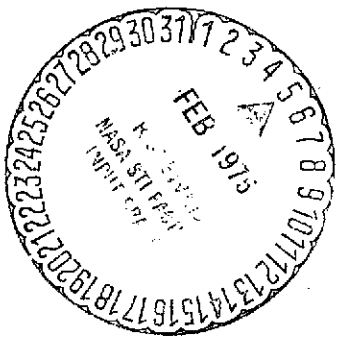

NATIONAL AERONAUTICS AND SPACE ADMINISTRATION

LANGLEY RESEARCH CENTER, HAMPTON, VIRGINIA 23665

1. Report No.	2. Government Accession No.	3. Recipient's Catalog No.
NASA TM X-72632		

4. Title and Subtitle	5. Report Date
NORMAL INJECTION OF HELIUM FROM SWEPT STRUTS INTO DUCTED SUPERSONIC FLOW	January 1975
	6. Performing Organization Code
7. Author(s)	8. Performing Organization Report No.
Charles R. McClinton and Marvin G. Torrence	
9. Performing Organization Name and Address	10. Work Unit No.
NASA Langley Research Center Hampton, VA 23665	505-05-41-01
	11. Contract or Grant No.
12. Sponsoring Agency Name and Address	13. Type of Report and Period Covered
National Aeronautics and Space Administration Washington, D.C. 20546	Technical Memorandum
	14. Sponsoring Agency Code

15. Supplementary Notes

Interim release of material to be combined with additional material and converted to a formal publication by June 1975.

16. Abstract

Recent design studies have shown that airframe-integrated scramjets should include instream mounted, swept-back strut fuel injectors to obtain short combustors. Because there was no data in the literature on mixing characteristics of swept strut fuel injectors, the present investigation was undertaken to provide such data. This investigation was made with two swept struts in a closed duct at Mach number of 4.4 and nominal jet-to-air mass flow ratio of 0.029 with helium used to simulate hydrogen fuel. The data is compared with flat plate mounted normal injector data to obtain the effect of swept struts on mixing. Three injector patterns were evaluated representing the range of hole spacing and jet-to-freestream dynamic pressure ratio of interest. Measured helium concentration, pitot pressure, and static pressure in the downstream mixing region are used to generate contour plots necessary to define the mixing region flow field and the mixing parameters. Experimental results show that the fuel penetration from the struts is less, for all cases, than the flat plate results. But the mixing rate is faster, producing mixing length less than half that experienced on the flat plate.

17. Key Words (Suggested by Author(s)) (STAR category underlined)	18. Distribution Statement
Fluid Mechanics Turbulent Mixing Fuel Injectors Scramjet	Unclassified Unlimited

19. Security Classif. (of this report)	20. Security Classif. (of this page)	21. No. of Pages	22. Price*
Unclassified	Unclassified	57	$4.25

*Available from { The National Technical Information Service, Springfield, Virginia 22151
STIF/NASA Scientific and Technical Information Facility, P.O. Box 33, College Park, MD 20740

NORMAL INJECTION OF HELIUM FROM SWEPT STRUTS INTO DUCTED SUPERSONIC FLOW

By Charles R. McClinton and Marvin G. Torrence

SUMMARY

Recent design studies have shown that airframe-integrated scramjets should include instream mounted, swept-back strut fuel injectors to obtain short combustors. Because there were no data in the literature on mixing characteristics of swept strut fuel injectors, the present investigation was undertaken to provide such data. This investigation was made with two swept struts in a closed duct at a Mach number of 4.4 and nominal jet-to-air mass flow ratio of 0.029 with helium used to simulate hydrogen fuel. The data are compared with flat plate mounted normal injector data to obtain the effect of swept struts on mixing. Three injector patterns were evaluated representing the range of hole spacing and jet-to-free-stream dynamic pressure ratio of interest. Measured helium concentration, pitot pressure, and static pressure in the downstream mixing region are used to generate contour plots necessary to define the mixing region flow field and the mixing parameters. Experimental results show that the fuel penetration from the struts is less, for all cases, than the flat plate results. But the mixing rate is faster, producing mixing lengths less than half that experienced on the flat plate.

INTRODUCTION

Scramjet concepts under study at Langley have evolved from basic axisymmetric designs, such as tested under the Hypersonic Research Engine Project, to modular, airframe-integrated designs. (See refs. 1 and 2.)

These latter scramjets feature nearly square combustors with minimum surface area and thus, low cooling requirements and employ both external nozzle expansion and external inlet compression. However, a significant fraction of the inlet compression is accomplished by instream swept struts which span the combustor and provide a means of distributing the fuel throughout the large cross section of the engine.

Satisfactory performance from any scramjet configuration is dependent upon uniform distribution of the fuel. Fuel injection schemes for the annular combustors of axisymmetric scramjets were based on nonreactive wall injection results which have been reported in references 3 to 8, and were refined during the Hypersonic Research Engine Project. However, wall injection cannot provide adequate fuel penetration for the airframe-integrated scramjet design concept as discussed in detail in reference 1. Therefore, these scramjets must rely on the instream swept struts to inject the fuel. Fuel injection and mixing characteristics for this type of injector have not been experimentally studied and are not amenable to exact analysis, but predictions based on flat plate studies with and without reaction have been used for preliminary design.

The present work was performed to study the fuel-air mixing on a basic swept strut having the general characteristics of the modular, airframe-integrated scramjet and to compare the mixing with empirical predictions based on flat plate mixing results. Primary emphasis is placed on reducing or minimizing the mixing length because chemical kinetics considerations have shown that scramjet combustion is mixing dependent. Injector design variables studied were jet-to-free-stream dynamic pressure ratio, jet lateral spacing, and jet diameter to strut gap ratio. All reported tests were run at a free-

stream Mach number of 4.4 and used normal injection from opposite staggered holes located downstream of the strut shoulder.

SYMBOLS

A, B, C	coefficients used in equation 2
C_D	jet discharge coefficient (average of all jets in configuration)
D	jet diameter, cm
Gap	minimum distance between struts, cm
L	mixing length - to η_{mix} = .95, cm
M	Mach number
$\dot{m}$	mass flow rate, kg/sec
P	jet penetration, cm
p	pressure, N/m^2
q	dynamic pressure, N/m^2
Q_R	ratio of jet dynamic pressure-to-inviscid undisturbed air dynamic pressure at the jet station
R_N	Reynolds number (free-stream condition based on strut gap, Gap)
S	jet spacing, cm
V	velocity, m/sec
x	streamwise coordinate, cm (see fig. 4)
y	lateral coordinate, cm (see fig. 4)
z	vertical coordinate, cm (see fig. 4)
z_1	edge of stream tube at jet station, cm (see fig. 2)
z'	edge of stream tube at survey station, cm (see fig. 2)

α	mass concentration
β	injection angle
Γ	ratio of integrated mass flow rate to measured injected mass flow rate
δ	boundary layer thickness, cm
δ^*	boundary layer displacement thickness, cm
η_{mix}	mixing efficiency
Λ	strut sweep angle
ρ	density, $\frac{kg}{m^3}$
ϕ	simulated equivalence ratio, $(\dot{m}_{He}/\dot{m}_{air}/0.0295)$

Subscripts:

∞	free stream tunnel condition
air	air
He	helium gas
j	jet condition
max	maximum value in mixing region
t	total condition
W	tunnel wall condition

TEST CONFIGURATION PHILOSOPHY

A sketch of the swept strut model is presented in figure 1. Two identical hollow struts were used throughout this investigation and the injector pattern on the struts was the test variable. Details of injector geometry will be discussed in a subsequent section. The remainder of this section will consider the philosophy used in selecting the injector geometry and test conditions.

Strut Selection

The strut geometry used in this investigation was a simple diamond cross section with wedge and sweep angles similar to current modular scramjet concepts (see ref. 1).

The strut thickness and contraction ratio selected produced strut leading-edge shock wave cancellation on the opposite strut shoulders at the design free-stream conditions. Shock and expansion wave locations were calculated for both design and off-design conditions by an updated version of the swept shock wave program described in reference 2.

Injector Selection

With tunnel size, strut geometry, and tunnel freestream conditions specified, preliminary fuel injector design parameters (i.e., jet location, injection angle, jet-to-free-stream dynamic pressure ratio, jet spacing, and jet diameter) were determined based on flat plate mixing results (see refs. 3 to 8). Important characteristics considered in injector selection include: good fuel distribution, both penetration and spreading; rapid mixing; and fuel equivalence ratio. All jets are sonic to simplify fuel delivery systems.

Fuel injectors are located directly downstream of the strut shoulder near the minimum width where required penetration is smallest and as far upstream as possible to reduce the combustor length. Normal or angular injection is preferred to coaxial injection at high combustor Mach numbers because faster initial mixing rates are obtained. Reference 3 showed that better performance (penetration and mixing rate) was obtained by angular (downstream) injection; however, for these tests only normal injection is used because of the large

quantity of comparable flat plate data.

Jet diameter sizing is based on the penetration results (see ref. 5) of single normal jets on a flat plate. To obtain a good fuel distribution, an opposite staggered jet pattern is used, as shown in figure 2(a). Considering the shape of the superimposed single jet mixing regions shown on this figure, a jet of sufficient size is selected so that the point of half maximum concentration (see fig. 2(b)) is located on the centerline between the struts. Thereby, the lower concentration in the outer edge of one jet mixing region is reinforced by the low concentrations in the lower sides of the mixing regions from the two opposite adjacent jets. For basic flat plate type normal injection, the injectant obtains most of its penetration at the jet station. In the downstream region the edge expands by turbulent diffusion, but the bulk penetration remains nearly constant. Downstream of the strut trailing edge the flow expands, complicating the penetration comparison to the flat plate configuration. A method suggested in reference 5 to compare penetration for these two cases is not affected by these geometry differences. The quantity of air in the flat plate single jet mixing region under $\alpha_{He} = 1/2\ \alpha_{He,max}$ (see fig. 2(b)) is used to determine the size of the undisturbed air stream tube at the jet station used for mixing. The height z_1 of this stream tube corresponds to 1/2 Gap in the strut model. Values of z_1/D from reference 5 suggest that for the current tests $3 \leq (Gap/D) \leq 5$ is appropriate for good fuel penetration. A range of jet diameters is considered because in addition to controlling fuel penetration, the jet diameter must also be correlated, through the continuity equation, with jet spacing and dynamic pressure to assure that the desired equivalence ratio is maintained. Therefore, the above range of Gap/D is a variable in the continuity equation

$$\phi = \frac{\left(\frac{\pi C_D}{4}\right) Q_R}{.0295\left(\frac{1}{2}\right)\left(\frac{S}{D}\right)\left(\frac{Gap}{D}\right)\left(\frac{V_j}{V_\infty}\right)} \tag{1}$$

Before solving equation (1), values must be selected for the dynamic pressure ratio Q_R and the jet spacing S/D.

Selecting values for Q_R and S/D is accomplished using the mixing efficiency parameter η_{mix} (see ref. 6). At any downstream station η_{mix} is defined as the fraction of the injected fuel that would burn if complete chemical reaction occurred without further mixing. The following mixing efficiency correlation was developed from data presented in reference 6 and other unpublished flat plate results:

$$\begin{aligned} \eta_{mix} &= A\left(\frac{x}{D}\right)^B Q_R{}^C \\ A &= 0.109 + 0.0301\,\frac{S}{D} \\ B &= 0.271 - 0.00976\,\frac{S}{D} \\ C &= -0.534 + 0.0347\,\frac{S}{D} \end{aligned} \tag{2}$$

Equation (2) is a useful tool in relating cold and hot mixing studies. In most scramjet applications supersonic combustion is mixing dependent. That is, fuel mixing is the controlling part of the combustion processes. For this type of combustion the mixing efficiency parameter obtained in cold tests has been shown to be nearly the same as the combustion efficiency parameter measured in hot tests.

Equations (1) and (2) were solved, assuming $\phi = 1.0$, $C_D = 0.75$, Gap = 2.30 cm and $V_j/V_\infty = 1.66$, producing the predicted mixing length to $\eta_{mix} = 0.95$ as functions of jet diameter (Gap/D), jet spacing, and jet-to-

free-stream dynamic pressure ratio shown in figure 3. The solid lines in this figure represent constant jet diameter solutions and the dashed lines represent constant dynamic pressure. First, the lowest jet-to-free-stream dynamic pressure possible for a sonic jet is somewhere on the order of $Q_R = 0.5$. Second, the spacing between adjacent jets must be less than 8 to 9 jet diameters to insure merging of adjacent jets at far downstream stations. The horizontal cross hatch region at S/D = 8.5 represents this limit. The last limit was discussed previously, the ratio of Gap/D. This limit is represented by the area within the shaded region. Considering these three limits, the flat plate prediction indicates that optimum injector design (minimum combustor length, L/Gap) incorporates the lowest jet-to-free-stream dynamic pressure ratio which produces sonic flow (about 0.5) and a value of Gap/D < 4.2, with jet spacing less than four diameters.

Hydrogen Simulation

Because of hazards involved in testing with large flow rates of hydrogen, helium was chosen as a substitute gas. Previous cold-mixing studies (ref. 8) have shown that the penetration and mixing rate of hydrogen and helium are nearly the same when the jet-to-free-stream dynamic pressure ratios are the same.

These results, with helium injection, represent the results expected for hydrogen injected at the same dynamic pressure ratio Q_R and mass flow ratio $\dot{m}_j/\dot{m}_{air}$ from jets at the specified spacings S/D and Gap/D.

TEST APPARATUS AND PROCEDURES

Tests were conducted in a 7.62 by 15.24 cm Mach 4.4 blowdown wind tunnel.

Two identical hollow struts were mounted vertically (see fig. 1) in the test section by two end plates flush mounted in the tunnel top and bottom walls. Both end plates anchored the struts and, in addition, the top plate served as a cap for the fuel settling chamber. Figure 1, cross section B-B, shows a sectional view of the strut top end plate bolted (bolts not shown) to both the top of the tunnel (forming the fuel settling chamber) and the two struts. Strut details are shown in cross section A-A. The strut design used was symmetrical with 4° half wedge angles (in the plane of the free-stream flow velocity) for leading and trailing edges and a sweep angle of 48°. Each strut has sufficient internal fuel flow area so that the maximum fuel Mach number is 0.30, producing a 1.5 percent fuel pressure loss through the strut from the settling chamber pressure. For all configurations tested, fuel injectors with D = 0.64 cm were located 1.28 cm downstream of the strut shoulder.

Tunnel and strut instrumentation consists of various static pressure orifices and total temperature and pressure measurements for the air and jet flows. Tunnel static pressure orifices (1.0 mm diam.) are depicted by dots on the sketch in figure 4. One row of static orifices runs along the tunnel and diffuser side wall centerline. In the vicinity of the struts these orifices are spaced at 1.28 cm intervals. The other row of orifices is on the tunnel side wall at x/Gap = 0, parallel to the strut shoulder. In addition, static orifices are located in the strut base plate between the struts. Static pressure measurements on the struts were made using solid dummy struts with pressure orifices located on both sides along the z = 7.62 cm line. Tunnel total pressure and temperature were measured in the 0.406 meter diameter pipe section ahead of the tunnel settling chamber and the jet total pressure and temperature were measured in the helium

settling chamber. As a check, the jet total pressure was also measured in the bottom of one strut.

The coordinate system is a floating origin rectangular system referenced to the 48° swept plane with x measured downstream from the strut shoulder, y measured across the tunnel from the centerline between the struts and z measured from the tunnel floor.

Three injector geometry configurations were selected for testing. A summary of geometry and test conditions for these configurations is presented in figure 5. Free-stream conditions and jet diameter are the same for all conditions. Free-stream Reynolds numbers presented are based on the strut gap (2.3 cm). The variables between the three configurations are jet spacing and dynamic pressure. For each successive test the number of jets is doubled and the jet dynamic pressure and jet spacing is cut in half. Configuration I, designed to operate at a jet-to-free-stream dynamic pressure ratio of 2, was run at 1.4 as will be discussed later.

Helium was supplied from a trailer to the fuel settling chamber by the supply system shown in figure 6. The pressure regulators were preset so that the helium flow was controlled by actuating the ball valve shown.

Pitot-gas sampling probe and static probe rakes used to survey the helium-air mixing region are shown in figure 7. The probe rake has the same sweep angle as the struts so all probe tips are at a constant x. The rake is moved across the tunnel ($\pm$ y-direction). The pitot-gas sampling probe is an internal expansion type with a tip ID of 0.3 mm expanding to a tube ID of 1.0 mm. Both calculations and actual measurements indicate no flow field interference exists between adjacent pitot probes within the range of flow conditions measured. But, this is not the case for the static probe rake

using conventional static probes. The interference problem combined with poor static pressure measurements made in the flow field between the struts with a conventional static probe, led to the development of the static probe design shown in figure 7. These probes, developed by Pinckney (ref. 9), are shorter and less susceptible to errors from misalignment.

As mentioned above, the pitot probe is also used to collect gas samples by the gas sampling system shown in figure 6. Each probe is attached by a short length of tubing and solenoid valve to a sample collection bottle. The transducers to measure pitot pressure are connected into the line between the pitot probes and sample bottle control valve. The contents of the sample bottles are analyzed on a process gas chromatograph for helium, nitrogen, and oxygen volume fractions.

The same general procedure is followed for both pitot and static probe surveys. For each survey the tunnel flow is established and a no injection data scan taken before helium is injected. After actuating the helium ball valve, the jet flow requires approximately two seconds to become steady. Data are taken as soon as the flow is steady. To take gas samples the evacuated sample bottles (open to the vacuum reservoir) are open to the pitot probes. After two or three seconds purge of the pitot probe connecting tubing and bottles, the downstream solenoid valves (fig. 6) are closed and the bottles are allowed to fill for seven to ten seconds before the upstream solenoid valves are closed. This procedure produced acceptable repeatability of gas sampling results.

RESULTS AND DISCUSSION

Tunnel Calibration

Results of tunnel calibration are presented in figures 8 and 9. Figure 8 presents the tunnel Mach number distribution along the tunnel sidewall as determined from measured wall static pressures and tunnel total pressures.

Pitot and static surveys were taken at x/Gap = 1.91; the reduced Mach number profiles are presented in figure 9. These profiles show flow uniformity down to a value of z/Gap less than 2.0. Below this value, the flow is affected by combined disturbances from the tunnel boundary layer and from the step produced by the strut end plate cavity. A blank plate was used to cover the helium settling chamber during these tests but the strut end plate cavity was not filled because it was farther downstream and not expected to influence the calibrations.

Strut Flow Field

Solid dummy struts with static pressure instrumentation were installed next and the resulting flow field was surveyed to check the predicted strut flow field. Predicted tunnel wall and strut displacement thickness and shock diagram are presented in figure 10, along with non-dimensionalized theoretical and measured tunnel wall and strut static pressures.

The outer passage wall and strut pressures are shown above the air flow diagram and the center passage (between struts) below. These experimental data points substantiate the boundary-layer displacement thickness corrected inviscid prediction method. Boundary-layer spreading of the shock induced pressure rise, although not calculated, is about as expected (see ref. 10). Inviscid stream conditions in the numbered bays on the diagram are tabulated in the upper left-hand corner. Inviscid strut shoulder conditions for the center passage correspond to values for bay 2 in this chart.

Mach number profiles downstream of the struts (without injection), reduced from pitot and static pressure survey data, are presented in figure 11. Figure 11(a) presents profiles at constant height z/Gap at various downstream stations. These profiles indicate a region of low Mach number wake flow directly behind the struts x/Gap = 5.0 and a relatively uniform high Mach number flow in the center and side passages. Farther downstream, the wake section of the profile diffuses across the entire flow with the resulting flattening of the entire profile. Figure 11(b) presents profiles at a fixed downstream station x/Gap = 6 for various values of z/Gap. These profiles indicate the strut end effects (lower Mach number for low z/Gap) caused by the strut induced downflow being compressed against the tunnel floor. Surveys above z/Gap = 3.32 were unaffected and, therefore, not presented. Because methods of reducing the observed end affects would be applied in an actual scramjet design, the present test avoided the region below z/Gap = 2.5.

Jet Flow and Mixing Region Surveys

As discussed earlier, mixing results presented herein are obtained with a single strut geometry using three different injector patterns, as shown in figure 5. These patterns and test conditions were chosen to produce a mixing region bulk helium-to-air mass flow ratio of 0.0295. However, two factors caused a variation in the mass flow ratio. First, the assumed jet discharge coefficient C_D was not correct. Measured values of C_D are 0.93, 0.86, and 0.61 for configurations I, II, and III, respectively. Each jet had the same geometry (jet diam. and length) so the variation of discharge coefficient is believed associated with the helium flow inside the struts. The other factor was that configuration I could not be operated at the design value

of $Q_R = 2.0$ because the tunnel choked, apparently as a result of the jets separating the tunnel wall boundary layer. The actual helium-to-air mass flow for configurations I, II, and III are 0.0258, 0.0401, and 0.0298, respectively.

The helium-air mixing region was surveyed at x/Gap = 5.0, 7.2, 11.6, and 22.7. A minimum data point grid was chosen, shown in figure 12, which allowed cross plotting in both y and z directions with a minimum number of runs. Figure 12 is the tunnel cross section normal to the free-stream flow direction. The vertical dashed lines depict the upstream position of the struts. All points shown are at constant x/Gap. Pitot pressure, static pressure, and gas samples were obtained at each point on the grid, and because of the rapid data turn-around, additional points on the constant z-surveys could be added to supplement points in regions of steep or uncertain concentration gradients. The survey data were reduced by a computer program to obtain point values of helium mass fraction, helium mass flow rate, and air mass flow rate, which are cross plotted to produce the desired mixing region flow field contours presented in figures 13 to 17.

Helium mass fraction contours produced by the three injector configurations are presented in figures 13 to 15 at each of the four downstream stations surveyed. These contour plots represent the helium distribution on the plane normal to the free-stream direction, as in figure 12, with the view looking upstream. Each line in the contour plots represents a constant value of helium mass fraction, with the highest value depicting the center of a jet mixing region. Individual jet mixing regions are easily discernible for most of the contours, and the regions spread with downstream distance as expected. Configuration I contours (fig. 13) do not merge until after the x/Gap = 11.6 survey station. For the other configurations, merging is more rapid. The

vertical dashed lines and solid elliptical symbols on each contour plot represent the strut and jet locations, respectively. The location of the mixing regions relative to the jet at the four locations gives an indication of the flow turbulence downstream of the swept fuel injection struts. The struts produce, in addition to a three-dimensional shock expansion flow system, a down-turning of the entire flow so that behind the shocks the lower part of the flow is compressed. These contour plots all show an upward shift in the mixing region at the x/Gap = 11.6 station which is believed to be caused by the upward redistribution of the flow. The fuel penetration and the decay of the maximum concentration, or mixing rate, are obtained from these figures and will be discussed in detail in later sections.

Typical helium and air mass flow rate contours are presented in figures 16 and 17, respectively. These contours are used to calculate mixing efficiency and to determine the accuracy of flow survey procedure, both of which will be discussed in later sections.

Fuel Penetration

Unlike flat plate mixing studies, fuel penetration is not an easily or clearly defined parameter in confined mixing tests. Penetration is generally defined by the displacement of the outer edge of the mixing region P/D, but for a confined flow, such as this, the outer edge of the mixing region is obscured once the opposite jets merge. Penetration has also been defined as the displacement of the point of maximum concentration, but the location of the point of maximum concentration is strongly dependent on the flow field geometry and resulting mixing rates and direction. This strong dependence rules out comparison between flat plate and strut cases using this penetration

parameter. The few contours which do show the outer edge of the mixing region are used to produce the penetration results (solid symbols) shown in figure 18. Also shown, for reference only, is penetration to the point of maximum concentration. The solid symbols at the first station x/Gap = 5.0 show that jet dynamic pressure has the expected affect of increasing penetration. Increasing the dynamic pressure ratio from 0.5 to 1.4 more than doubles the penetration. However, all strut penetration values are much smaller than observed during flat plate mixing studies as shown in the following comparison:

Present Tests (x/D = 18)			Flat Plate, Reference 5 (x/D = 15)	
Configuration	Q_R	P/D	Q_R	P/D
I	1.4	2.65	1.5	5.4
II	1.0	1.67	1.0	5.1
III	0.5	1.18	0.5	4.0

In this table the present penetration is measured at x/Gap = 5.0 (x/D = 18) and the flat plate results are measured closer to the jet at x/D = 15. This poor penetration results from one or more of the following factors: (1) thin bounday layer $\delta/D < 0.5$ on the struts; (2) shock wave-jet interference; and (3) strut shoulder vortex-jet interference. Additional study in the initial mixing region is required to pinpoint the factors reducing the penetration.

Mixing Rate

Decay of the maximum secondary jet concentration has been used extensively as a measure of the rate of mixing. Although the mixing efficiency η_{mix} is a more useful parameter in discussing mixing rates, both will be presented, because some earlier results, as presented, cannot be converted to η_{mix}. Values of maximum concentration decay measured during flat plate mixing studies

are presented separately in figure 19(a) and are compared with the three injector configurations in figures 19(b) to 19(d). Solid lines on figure 19(a) represent the decay of maximum concentration for a single jet (ref. 5) and multiple jets with S/D = 12.5 (ref. 6). Dash lines represent the decay of the maximum concentration for multiple jet studies with S/D = 6.25 (ref. 6). Both cases exhibit smaller maximum concentration for lower values of jet-to-free-stream dynamic pressure. On the flat plate, jet spacing has a definite effect on the mixing rate. Closely spaced jets tend to mix faster initially but slower farther downstream. This characteristic is believed to result from the initial increased turbulence, particularly from the jet induced shock wave interference with the adjacent closely spaced jets; and then farther downstream the jet merging becomes predominant and restricts the mixing rate.

Maximum concentration decay for configuration I is presented in figure 19(b) with the flat plate results for the same jet spacing (12.5) and jet-to-free-stream dynamic pressure ratio (1.5). The rate of decay of the maximum concentration is about the same as the comparative flat plate case shown, but the initial helium concentration is lower. Two factors could cause this lower concentration: the low bulk helium-to-air mass flow ratio (0.0258), and the increased turbulence typical to the strut flow field as compared with flat plate flow. The former would be a small effect, at most accounting for 1/3 of the difference.

Maximum concentration for configuration II, presented in figure 19(c), shows about the same rate of decay as the similar flat plate case S/D = 6.25, Q_R = 1.0 , but the initial value is higher. The bulk helium-to-air mass flow rate (0.0401) is higher than intended (0.0295) which tends to increase the maximum concentration measured.

The maximum concentration for configuration III, presented in figure 19(d), decays at a faster rate and has a slightly lower initial value than configuration II. Although there is no comparable flat plate data S/D = 3.13, Q_R = 0.5 , trends indicated by the other two spacings suggest that, on the flat plate, the initial mixing for this configuration should be fast $\alpha_{He,\ max}$ = 0.035 @ x/D = 30 and downstream mixing should be quite slow. But the initial value is considerably higher than α_{He} = 0.035 and the mixing rate faster than anticipated. The helium-to-air mass flow rate is 0.0298, nearly the design value.

Mixing Efficiency

Sample helium and air mass flow rate contours presented in figures 16 and 17, respectively, are integrated to determine helium and air flow rates necessary to calculate both the total measured helium flow and the mixing efficiency η_{mix} at each survey station. Mixing efficiency is defined as that fraction of the fuel that would burn ($\dot{m}_{fuel}/\dot{m}_{air} \leq 0.0295$) if complete chemical reaction occurred without additional mixing. For these tests the same definition of η_{mix} is used except helium mass flow replaces fuel. The actual procedure for calculating mixing efficiency is presented in the Appendix

Experimental mixing efficiency values are compared to the flat plate prediction in figure 20. The predictions, based on equation (2), are presented by the solid lines and the present data by symbols. Data point fairings are represented by the dashed curve topping the cross-hatched region. The cross-hatched region represents the possible error due to the computed deficiency of the helium measured in the mixing region. This error is discussed in the Appendix. Mixing is assumed complete when η_{mix} reaches 0.95. Figure 20 shows a considerable reduction in mixing length for the strut mixing compared

to the flat plate predictions. The flat plate prediction method gives the correct trend in mixing lengths, but each configuration tested required less than half the predicted mixing length. To assure that the reduced mixing length is not entirely due to known measurement errors, the maximum error curves show that the possible error in measured mixing length x/Gap is only a small fraction of the difference between predicted and measured.

The exact nature of the observed increased mixing rate is not certain. The mixing efficiency decays more rapidly both near the jet and farther downstream indicating that the cause is associated with the increased levels of turbulence in the strut flow field.

CONCLUDING REMARKS

A preliminary study has been conducted to determine the appropriate fuel injector pattern and the resulting mixing performance for a scramjet combustor featuring swept fuel injection struts. In addition, the injector performance was compared to flat plate injector performance. Helium was used to simulate the hydrogen fuel. Both the helium penetration and mixing length were less than flat plate mixing values. Of the three injector configurations tested, the fastest mixing required about 20 strut gaps of downstream length. This configuration represents the optimum design based on flat plate data correlations.

APPENDIX

As discussed in the text, the helium and air flow rate contours (figs. 16 and 17) are integrated to determine the bulk helium and air flow rates.

These values are used to determine the mixing efficiency η_{mix} and the ratio of the measured helium to the total helium injected Γ.

Mixing efficiency was defined in the text as that fraction of the fuel (helium) that would burn if chemical reaction were to occur without additional mixing. Determining the fraction of fuel that would react is accomplished by dividing the overall mixing region R into two parts, fuel lean Rl and fuel rich Rr. In the fuel lean $\phi < 1$ region, all of the fuel will react; in the fuel rich $\phi > 1$ regions, the quantity of fuel reacting is governed by the total air present. So, if the total helium in the mixing region is

$$\dot{m}_{He,\ R} = \int_R (\rho_{He} V_{He})\ dA \qquad \text{(A-1)}$$

the total helium that would react in the fuel lean region is

$$\dot{m}_{He,\ Rl} = \dot{m}_{He,\ R} - \int_{Rr} (\rho_{He} V_{He})\ dA \qquad \text{(A-2)}$$

where the integral represents the total fuel in the rich regions (see dashed curve, fig. 16). The total helium that would react in the fuel rich region is limited by the total air in that region, so

$$\dot{m}_{He,Rr} = 0.0295 \int_{Rr} (\rho_{He} V_{He})\ dA \qquad \text{(A-3)}$$

where the integral is the total air flow in the fuel rich area (see fig. 17) and 0.0295 is the mass ratio of H_2 to air for stoichiometric combustion. Using these relations the mixing efficiency is

$$\eta_{mix} = \frac{\dot{m}_{He,\ Rl} + \dot{m}_{He,\ Rr}}{\dot{m}_{He,\ R}} \qquad \text{(A-4)}$$

The flow field integration points out the problem associated with obtaining accurate gas concentration measurements in supersonic gas mixtures. The

total helium measured in the mixing region is some fraction Γ of the actual quantity present because of collection probe limitations. Values of Γ are presented in figure A1, along with typical values from previous flat plate normal injection studies. Values of Γ are typically lowest near the jet, but in the present studies they are extremely low near the jet and only approach 80 percent at the most downstream station. The high jet-to-free-stream dynamic pressure ratio configurations tend to have a smaller Γ than the low Q_R configurations. These results are consistent with previous results which indicate that Γ is related to the local level of turbulence. The mixing efficiency is the primary result of this study, so an attempt has been made to analyze the maximum error assuming that all concentration measurements are in error by a factor equal to Γ. By this analogy, the dashed "maximum error" curves on figure 20 were developed. These curves show that even with small Γ's the predicted mixing length has relatively small error. A more comprehensive procedure is being explored for compensating for the poor concentration measurements, but the method has not been completed at this time.

REFERENCES

1. Henry, J. R.; Anderson, G. Y.: Design Considerations for the Airframe-Integrated Scramjet. Presented at the First International Symposium on Airbreathing Engines, Marseille, France, June 1972.

2. Trexler, C. A.: An Experimental Investigation of the Forebody of a Hypersonic Inlet Model and a Comparison with Theory. M.S. Thesis in M.E., VPI&SU, April 1971.

3. McClinton, C. R.: The Effect of Injection Angle on the Interaction between Sonic Secondary Jets and a Supersonic Free Stream. NASA TN D-6669, 1972.

4. McClinton, C. R.: Effect of Wall Boundary Layer Thickness-to-Jet Diameter Ratio on Mixing of a Normal Hydrogen Jet in a Supersonic Stream. NASA TM X-3030, 1974.

5. Rogers, R. Clayton: A Study of the Mixing of Hydrogen Injected Normal to a Supersonic Airstream. NASA TN D-6114, 1971.

6. Rogers, R. Clayton: Mixing of Hydrogen Injected from Multiple Injectors Normal to a Supersonic Airstream. NASA TN D-6476, 1971.

7. Torrence, M. G.: Concentration Measurements of an Injected Gas in a Supersonic Stream. NASA TN D-3860, 1967.

8. Torrence, M. G.: Effect of Injectant Molecular Weight on Mixing of a Normal Jet in a Mach 4 Airstream. NASA TN D-6061, 1971.

9. Pinckney, S. Z.: An Improved Static Probe Design. AIAA Journal, Apr. 1974.

10. Pinckney, S. Z.: Semiempirical Methods for Predicting Effects of Incident Reflecting Shocks on the Turbulent Boundary Layer. NASA TN D-3029, 1965.

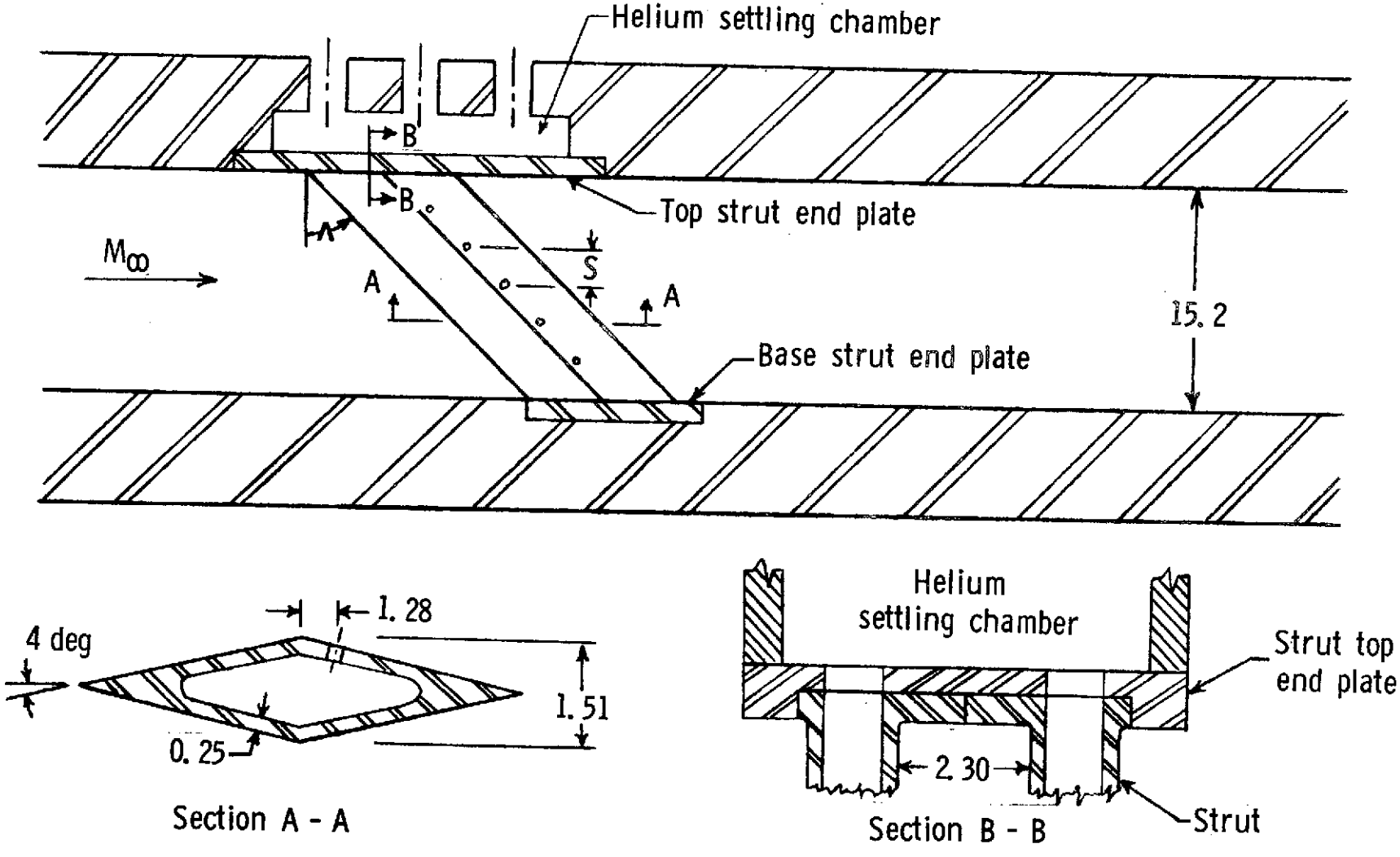

Figure 1. - Tunnel and strut details. All dimensions are in centimeters.

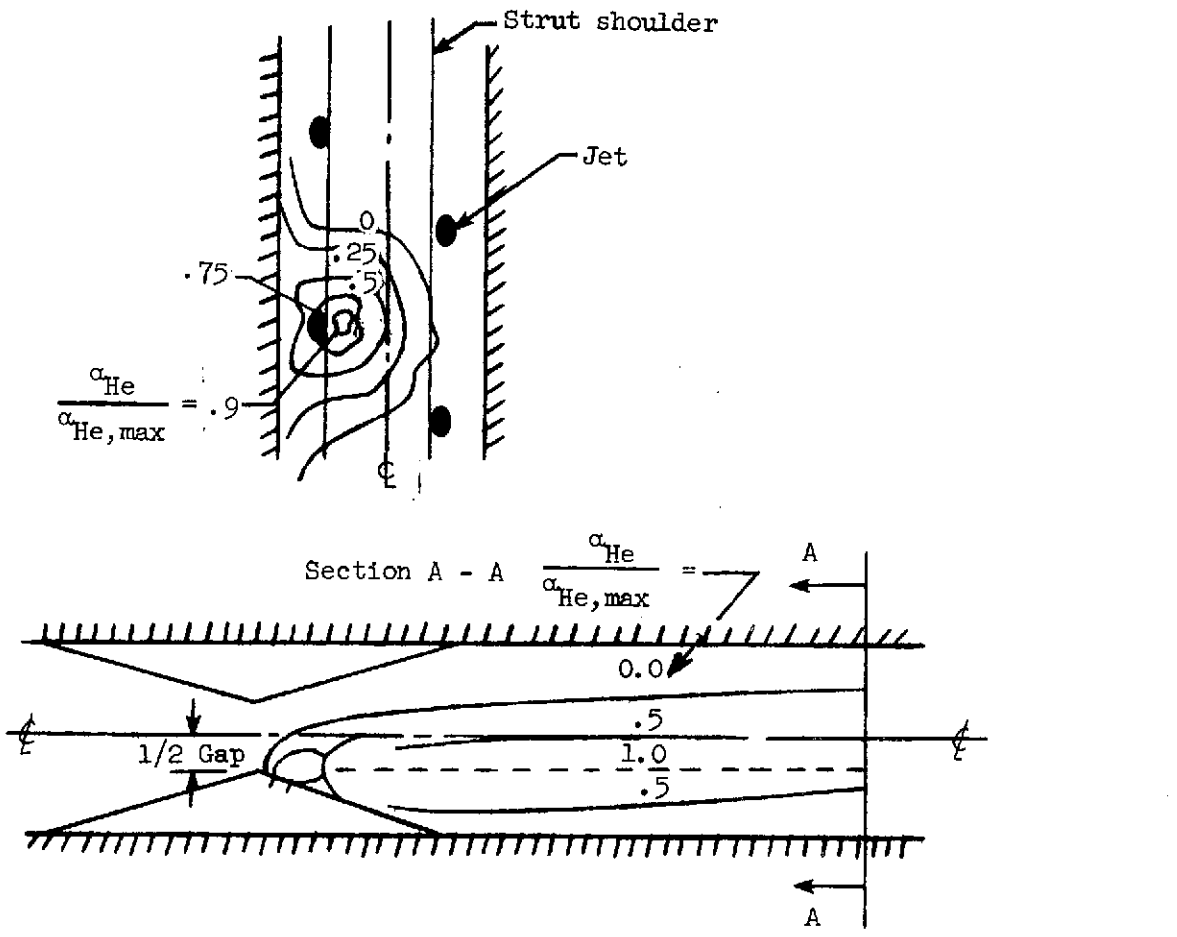

(a) Swept strut flow model .

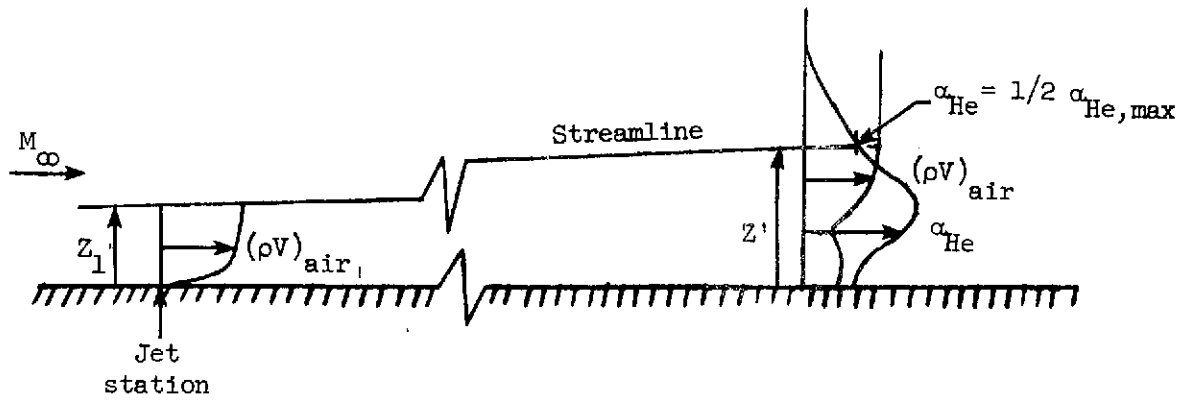

(b) Flat plate model.

Figure 2. - Jet diameter selection.

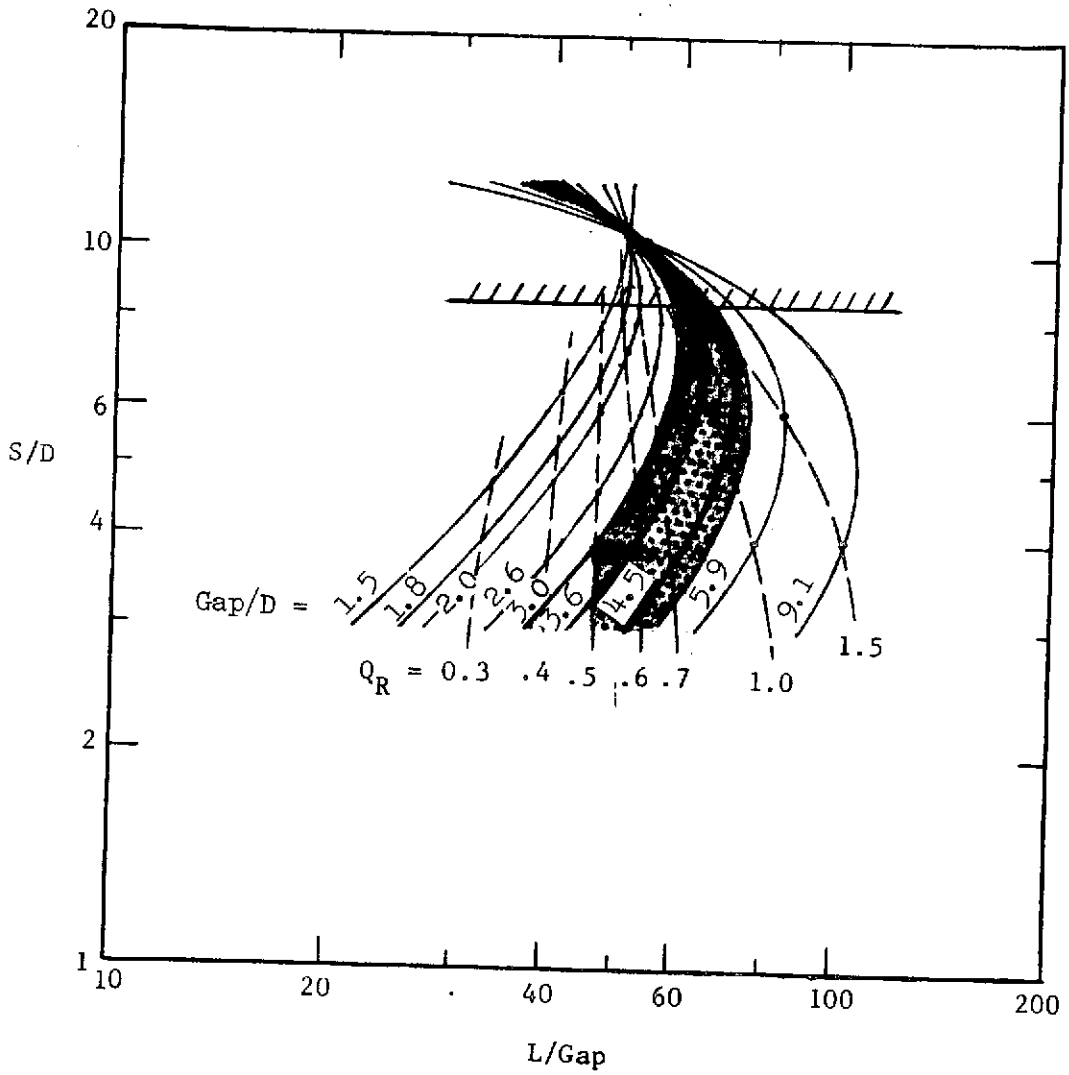

Figure 3.- Predicted mixing length to η_{mix} = .95.

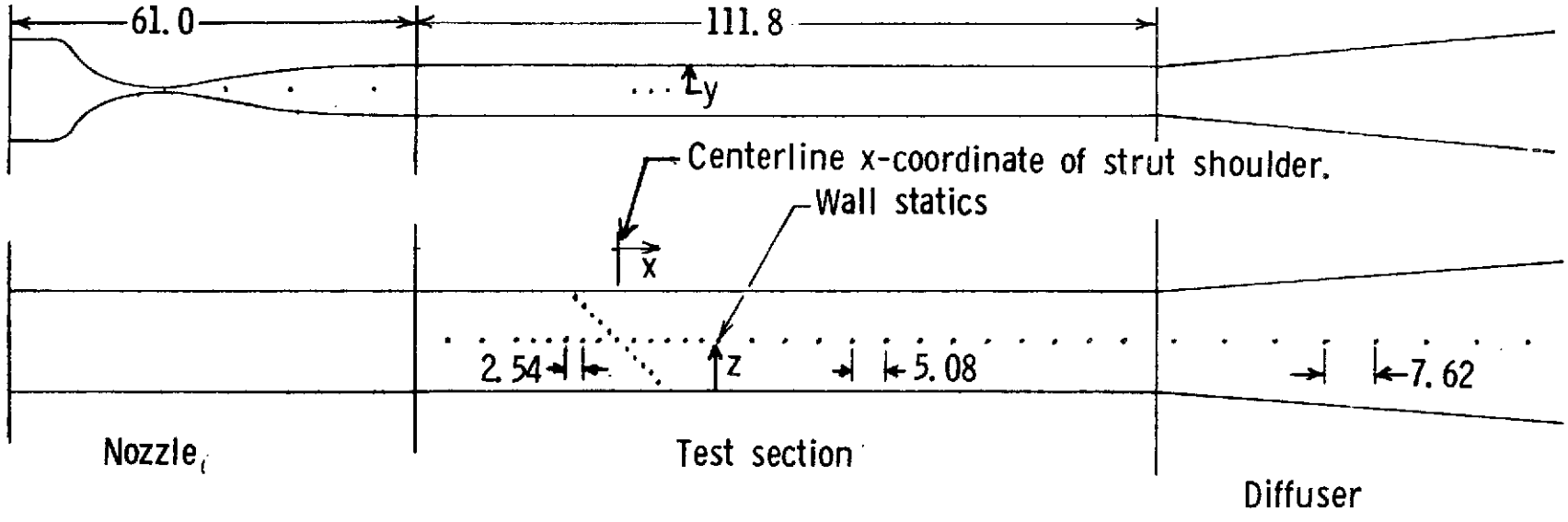

Figure 4. - Location of tunnel wall static orifices.

All dimensions are in centimeters.

	INJECTOR CONFIGURATION		
	I	II	III
M_j	1.0	1.0	1.0
S / D	12.5	6.25	3.13
D, cm	0.64	0.64	0.64
Q_R	1.4	1.0	0.5
$p_{t,j}$, N/m^2	1.197×10^6	0.855×10^6	0.4275×10^6
M_∞	4.4	4.4	4.4
$p_{t,\infty}$, N/m^2	3.896×10^6	3.896×10^6	3.896×10^6
R_N	3.327×10^6	3.327×10^6	3.327×10^6

Figure 5. - Test conditions.

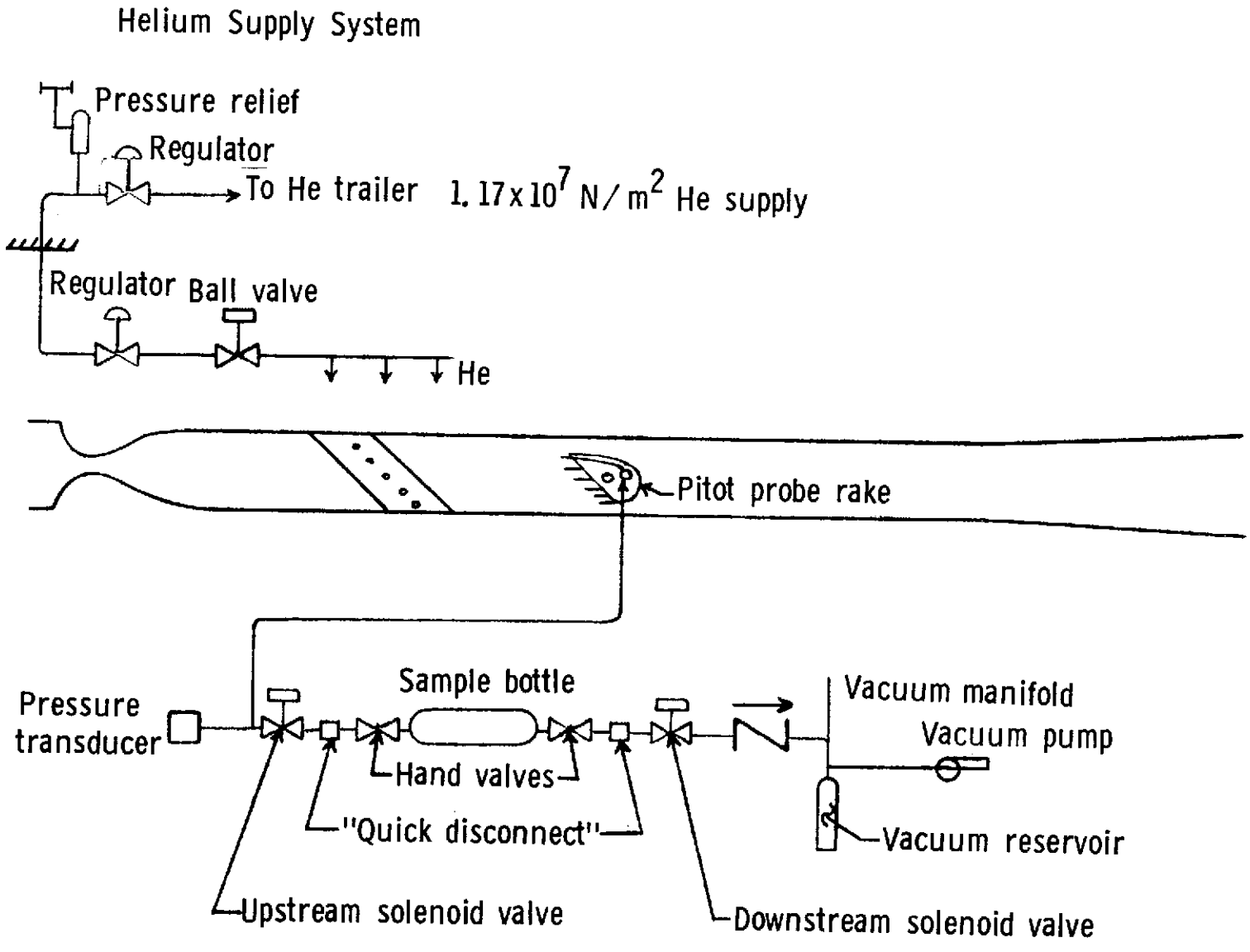

Typical Pitot - Gas Sampling System.

Figure 6. - Systems.

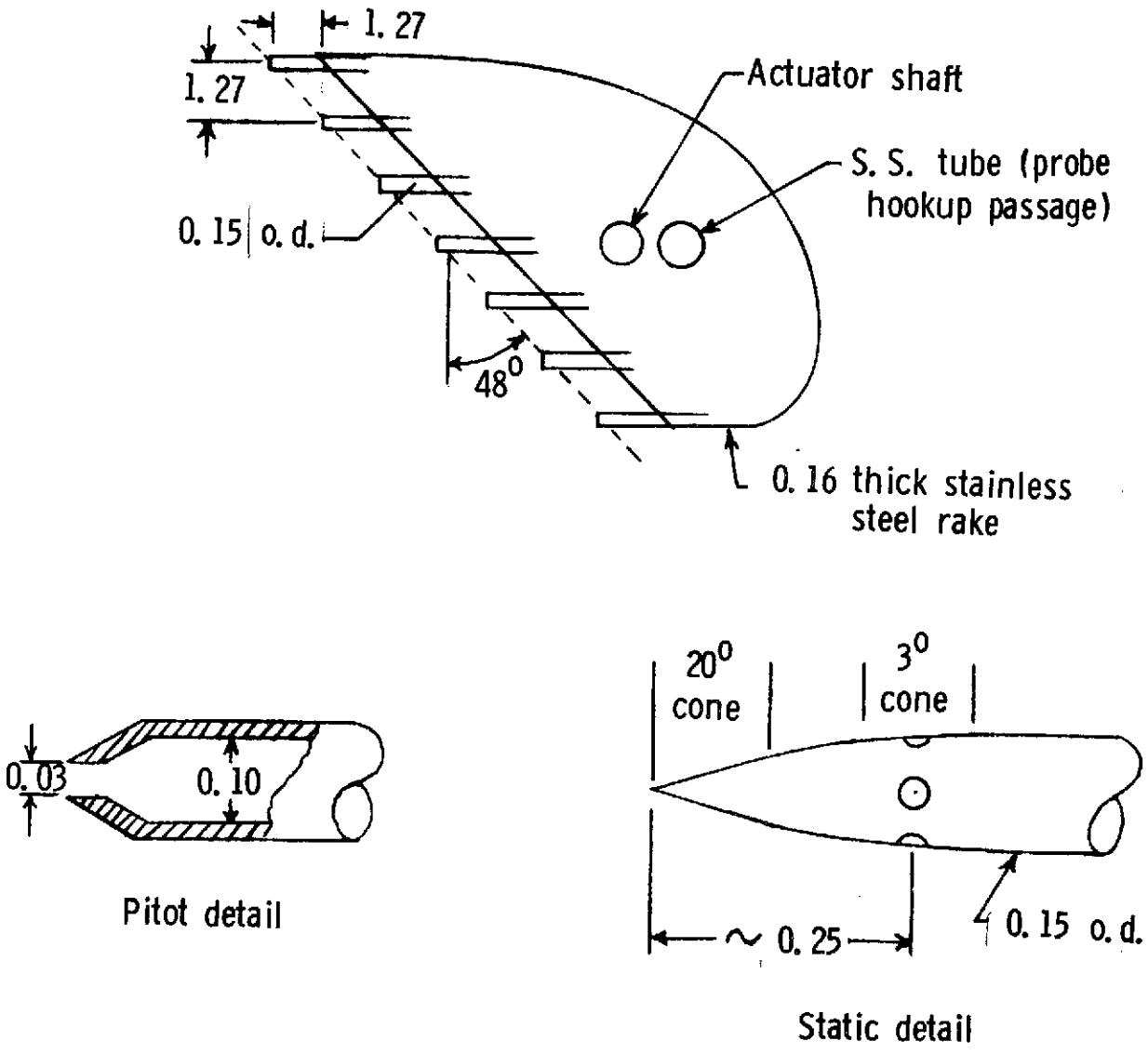

Figure 7. - Probe rake and details.

All dimensions are in centimeters.

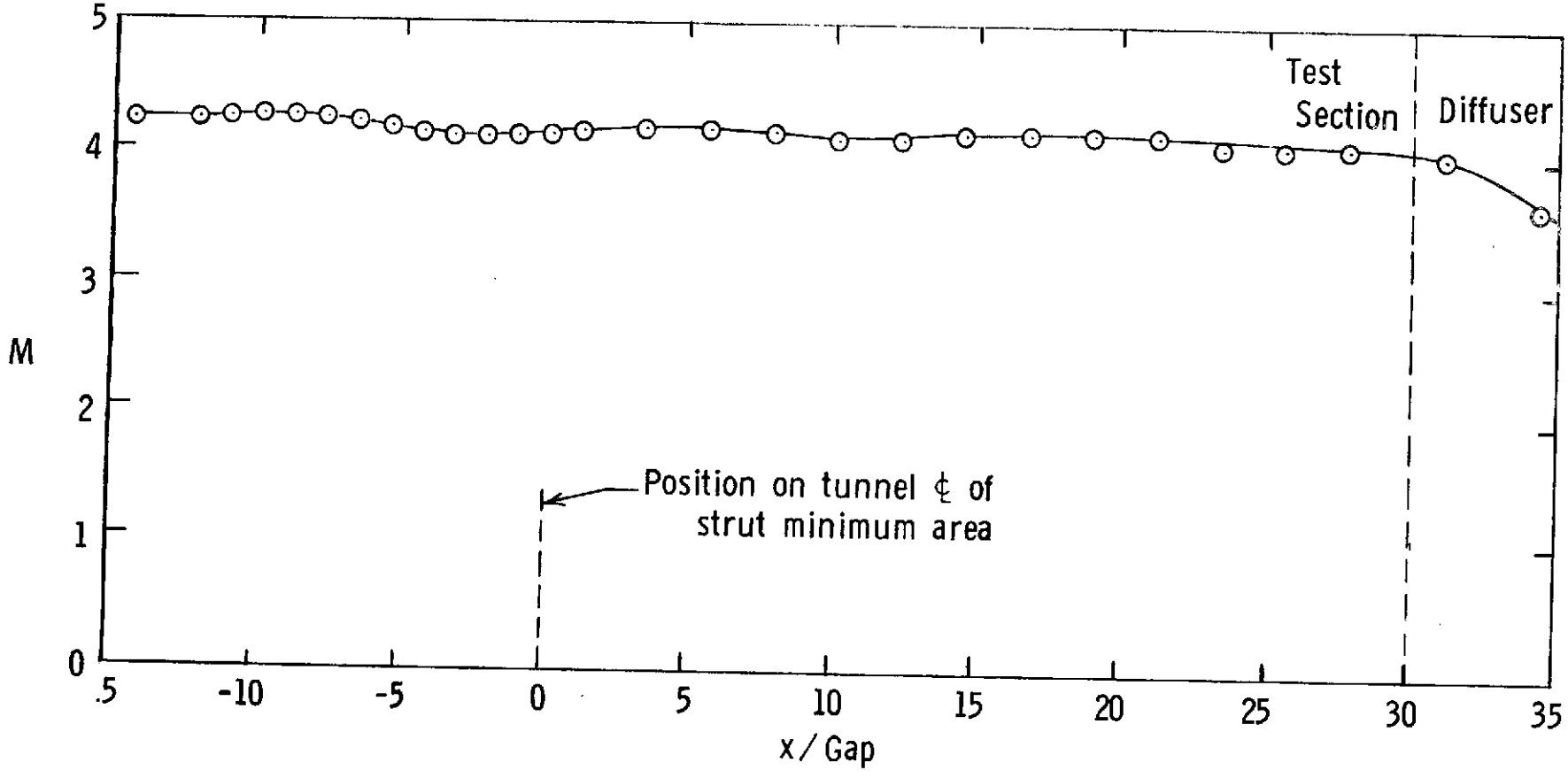

Figure 8. - Tunnel wall Mach Number based on $p_w/p_{t,\infty}$, $p_{t,\infty} = 3.861 \times 10^6$ N/M^2.

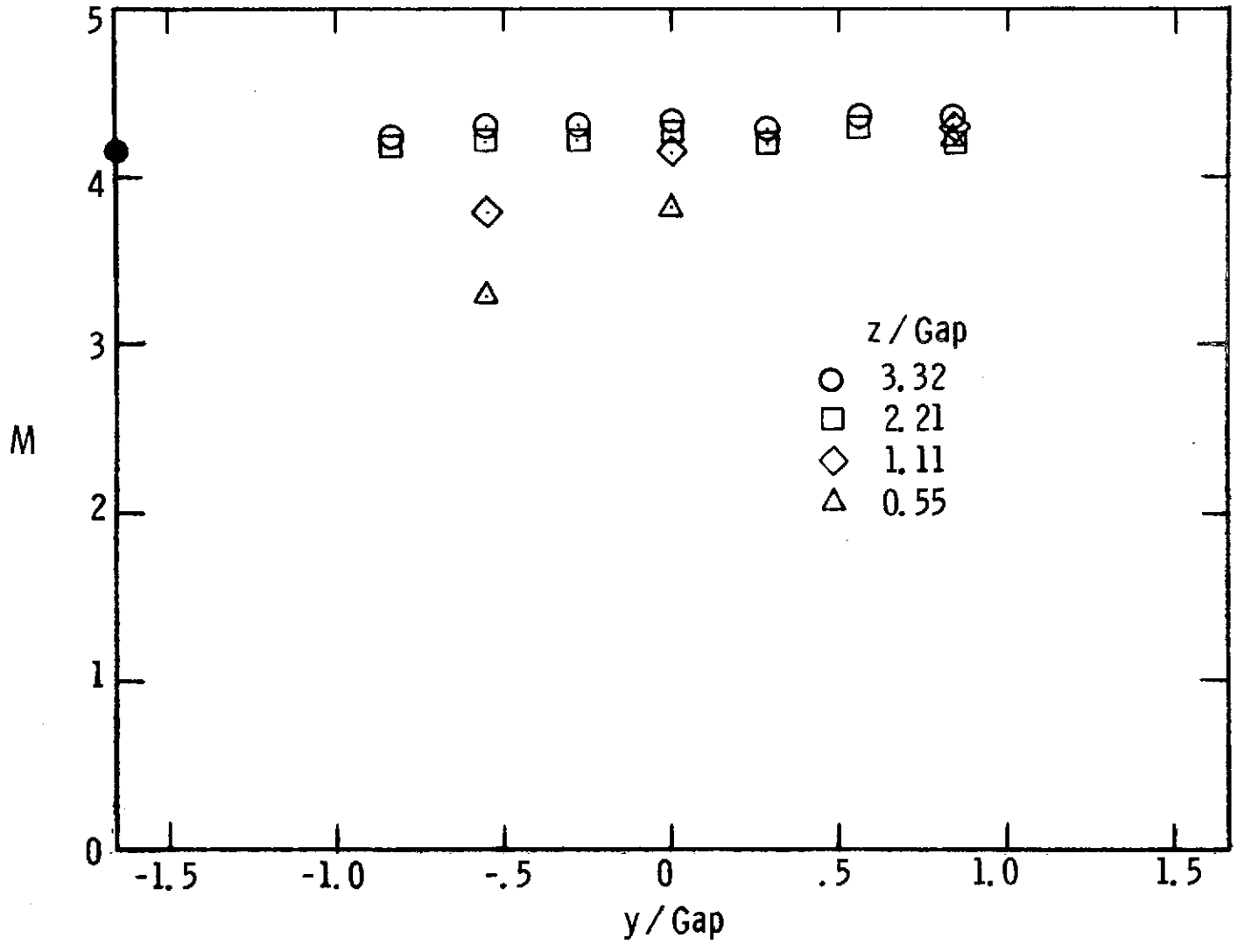

Figure 9. - Mach number profiles, no struts, x / Gap = 1.91.

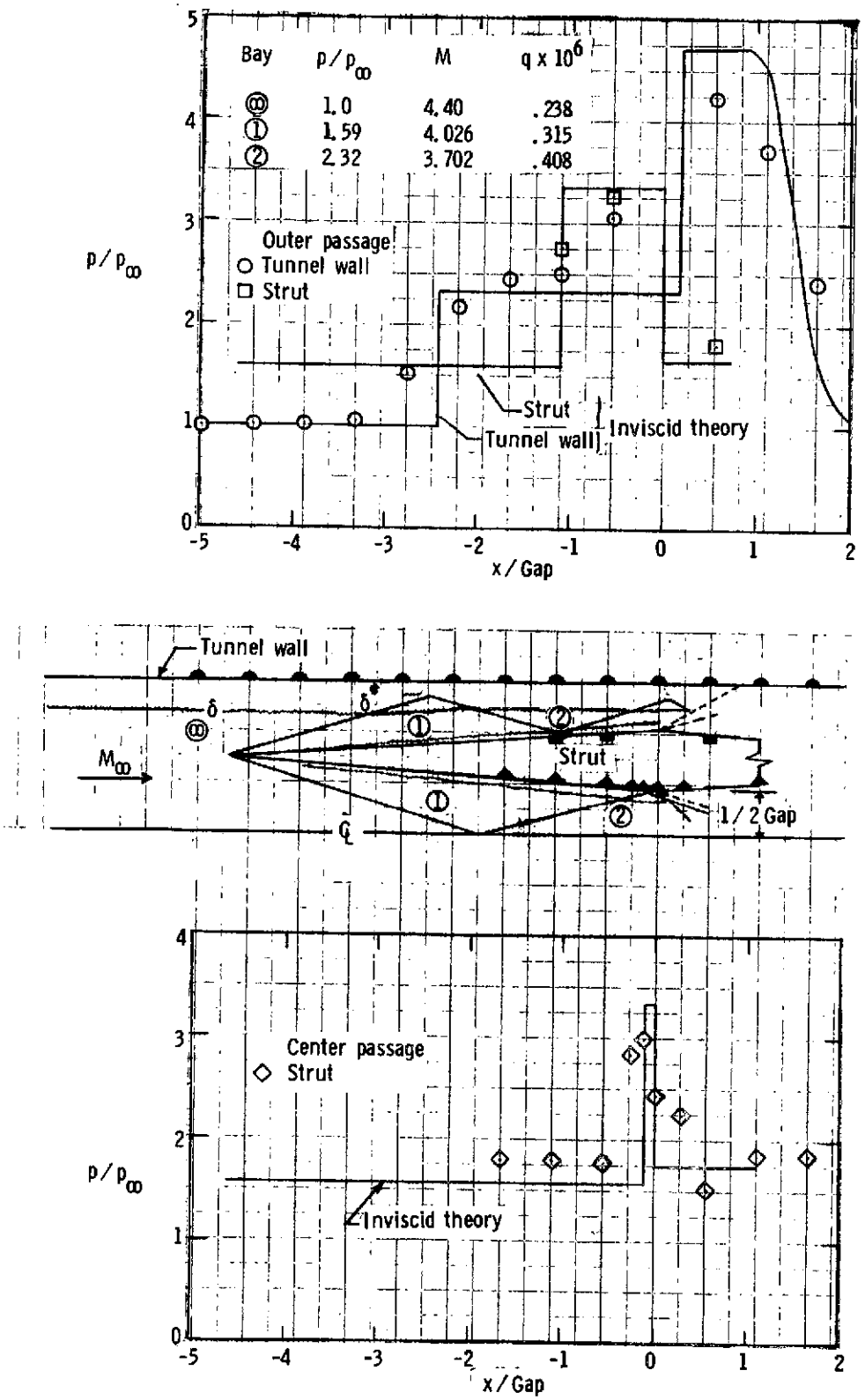

Figure 10. - Predicted strut flow and measured wall statics.

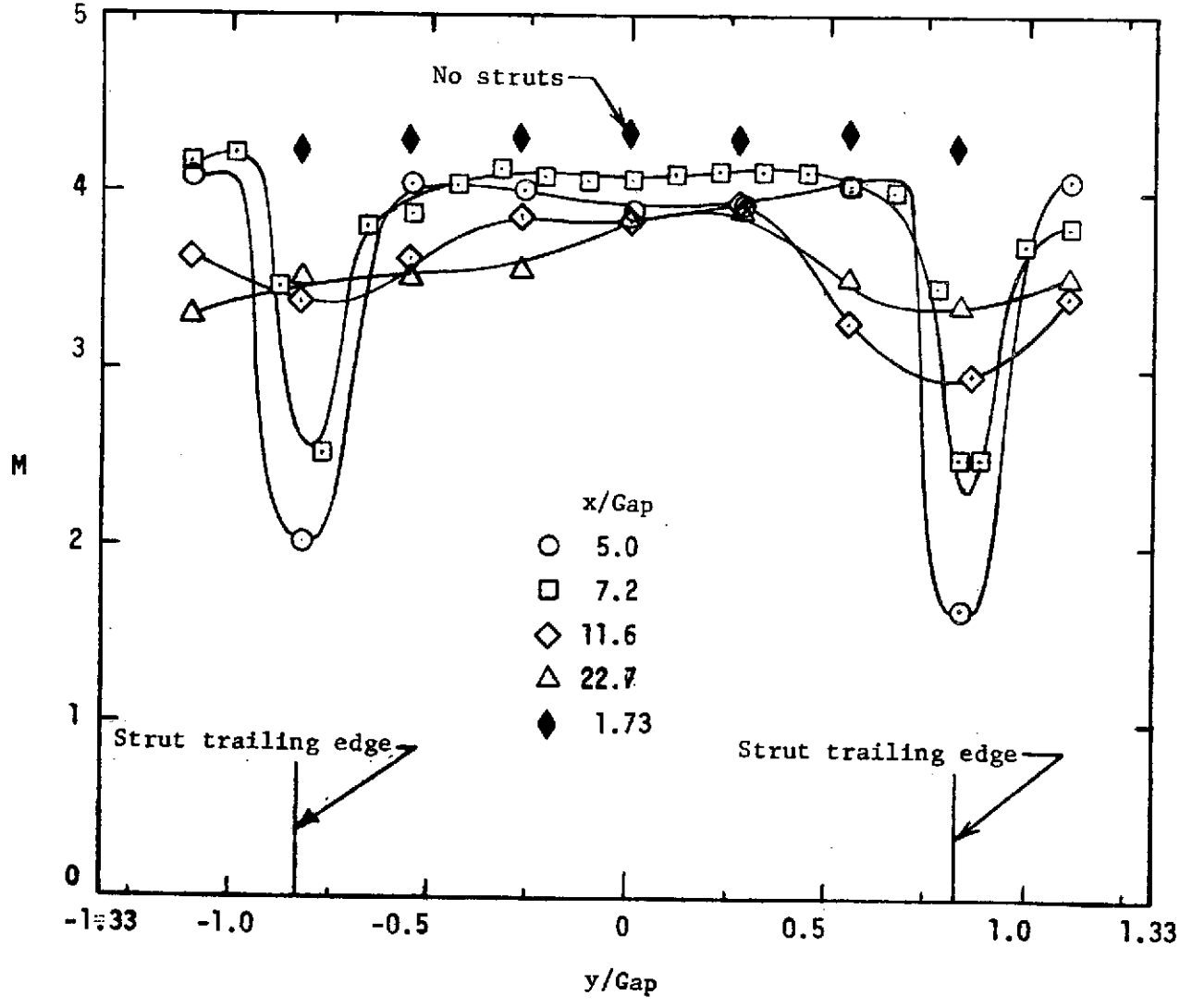

(a) Variation with downstream distance, z/Gap = 3.32.

Figure 11.- Mach number surveys, no injection.

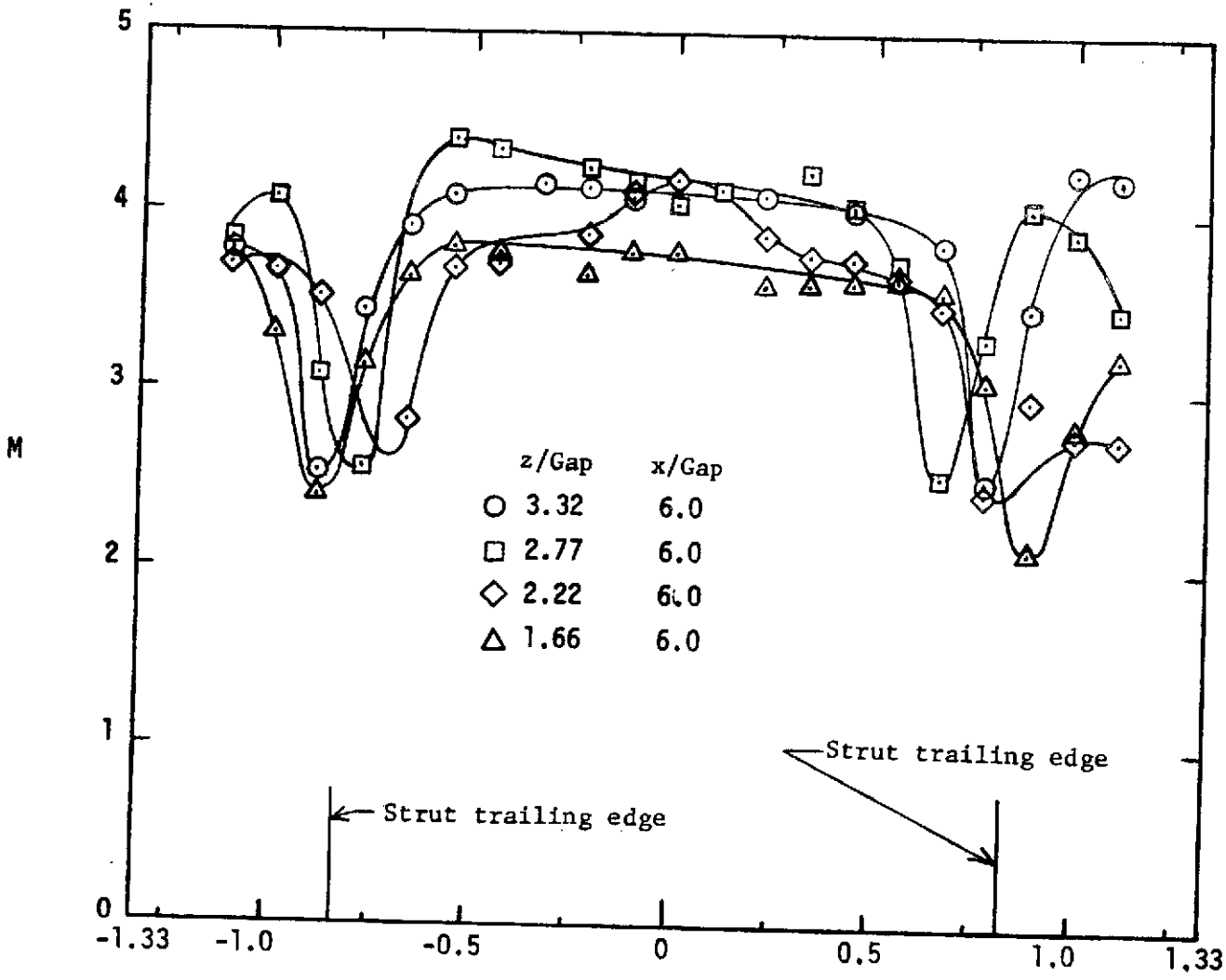

(b) Strut End Effects.

Figure 11.- Concluded.

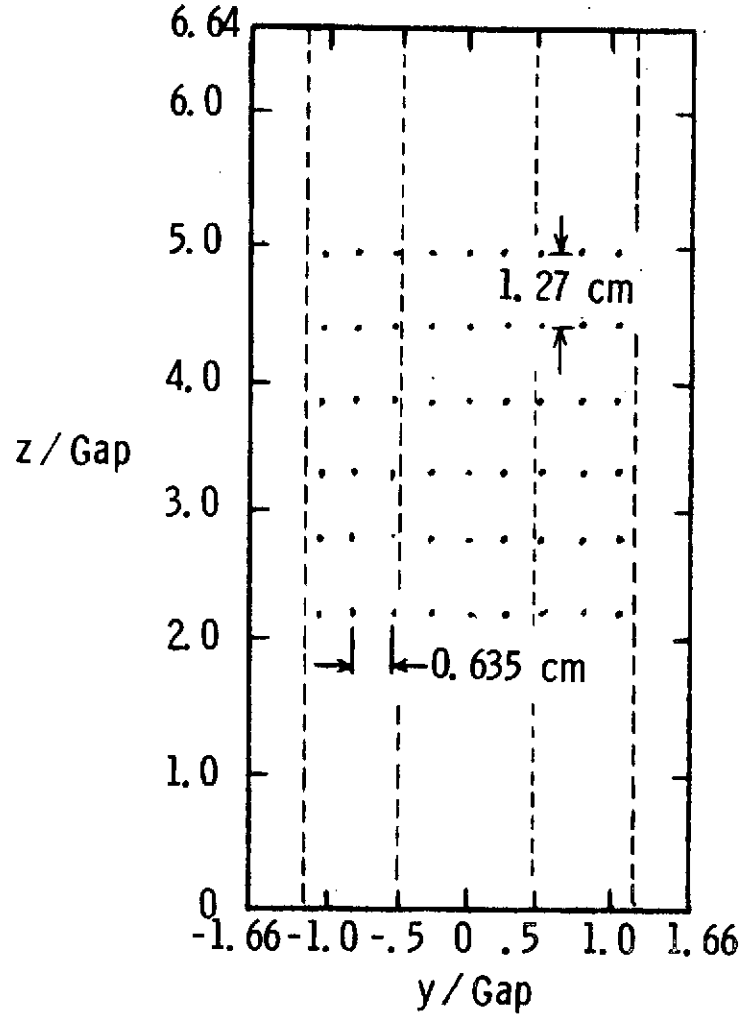

Tunnel cross section

Figure 12. - Minimum data point grid.

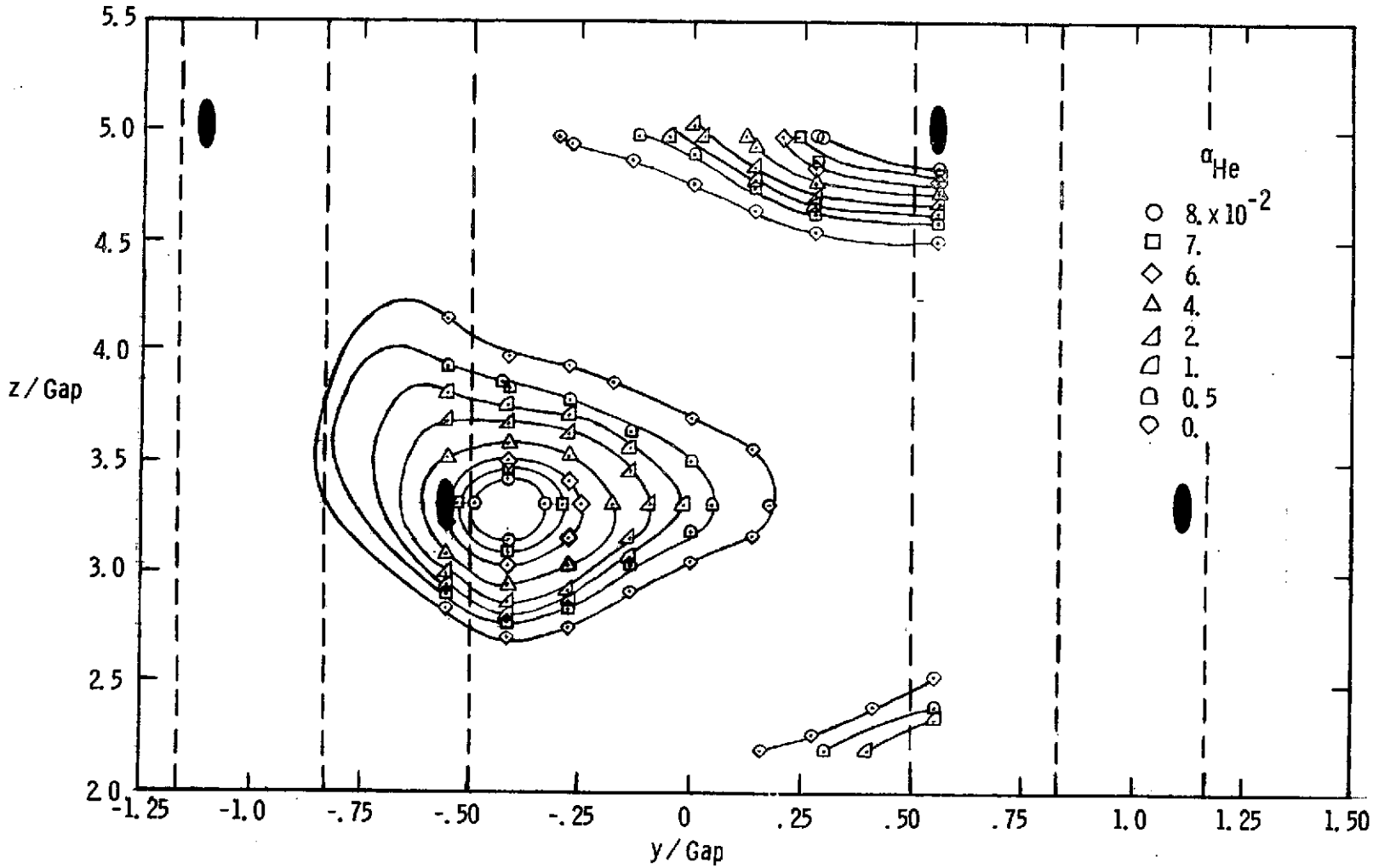

(a) x / Gap = 5.0

Figure 13. - Helium mass concentration contour, Configuration I.

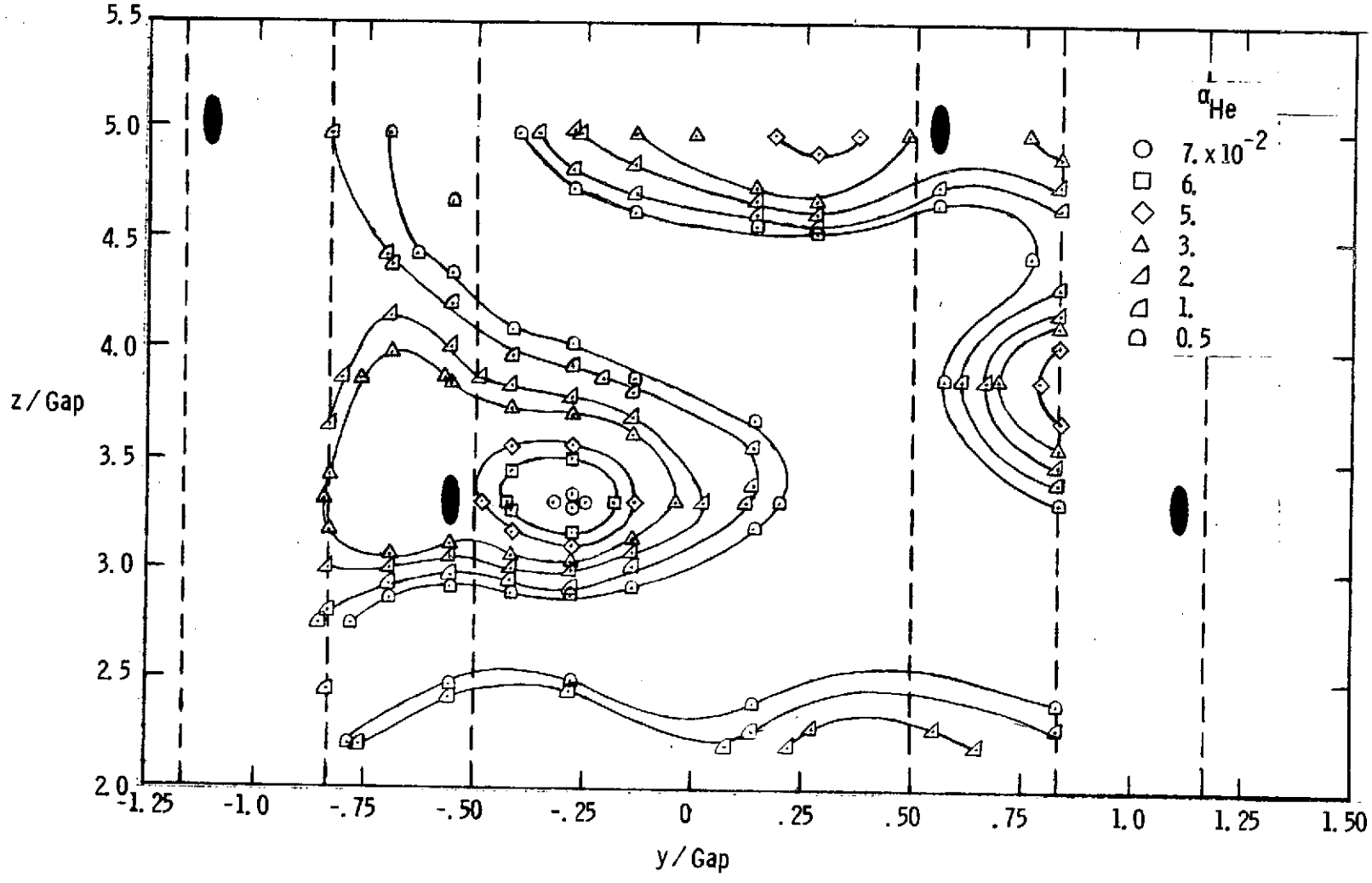

(b) x / Gap = 7.2

Figure 13. - Continued.

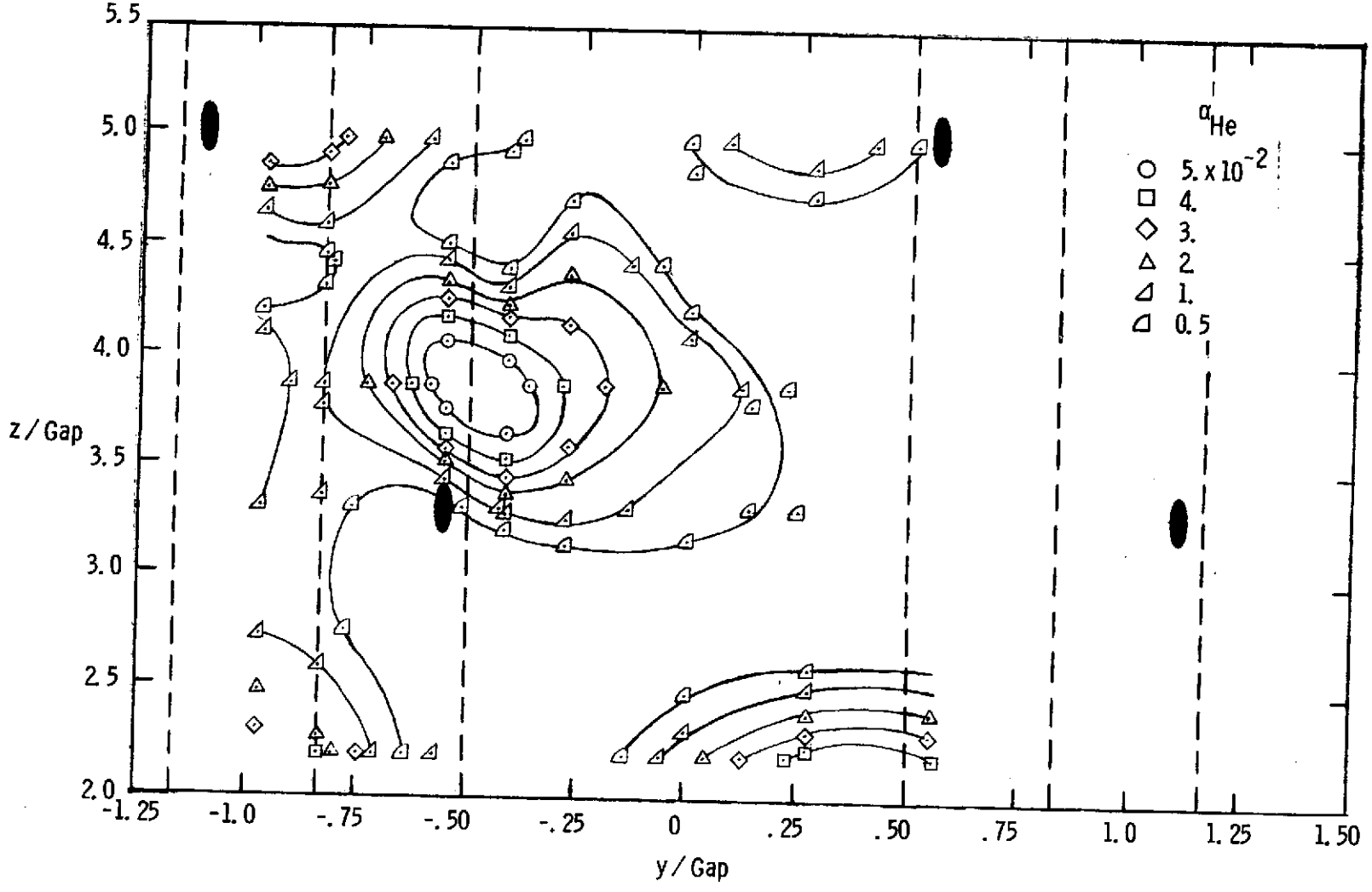

(c) x / Gap = 11.6

Figure 13. - Continued.

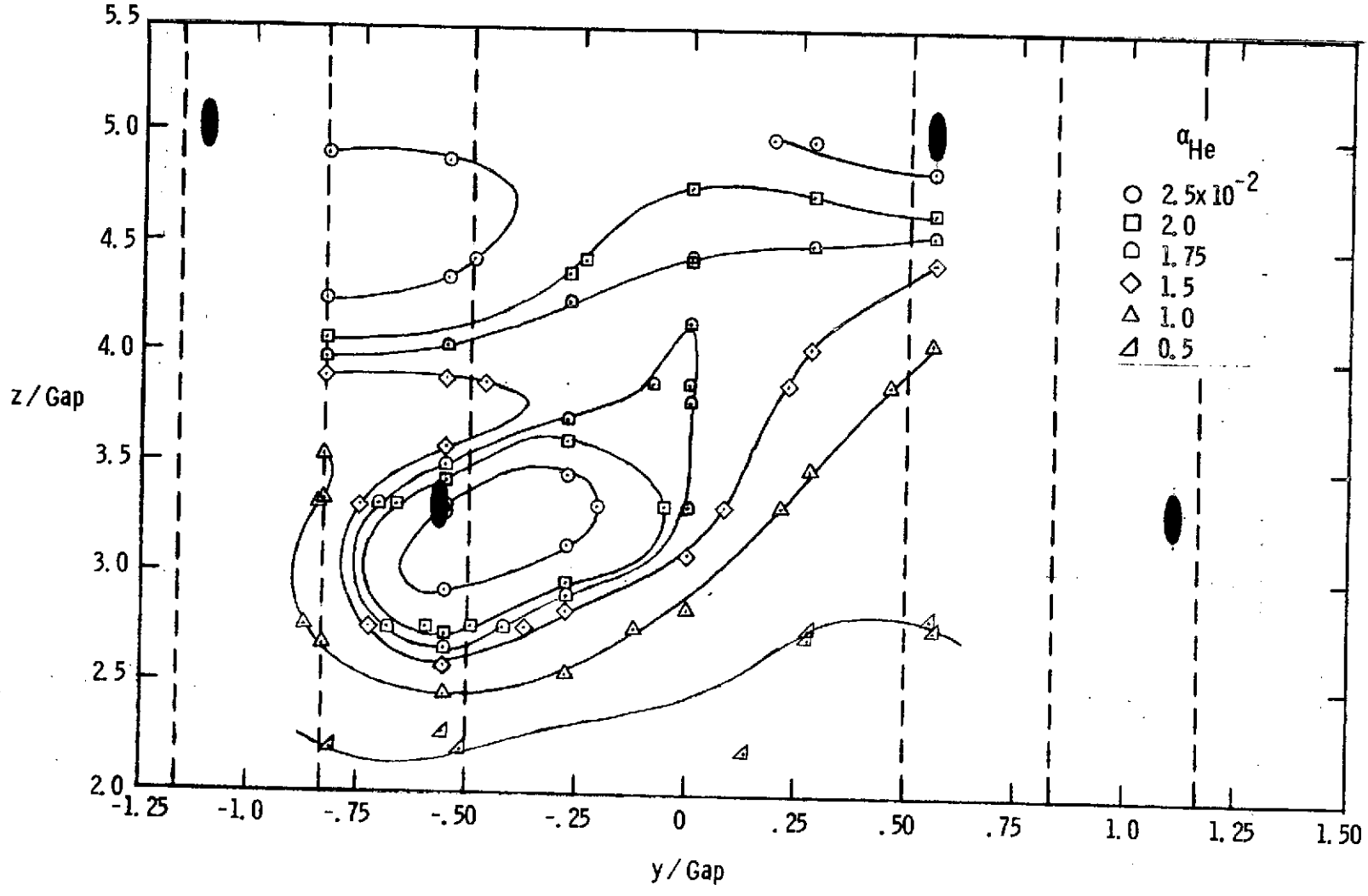

(d) x / Gap = 22.7

Figure 13. - Concluded.

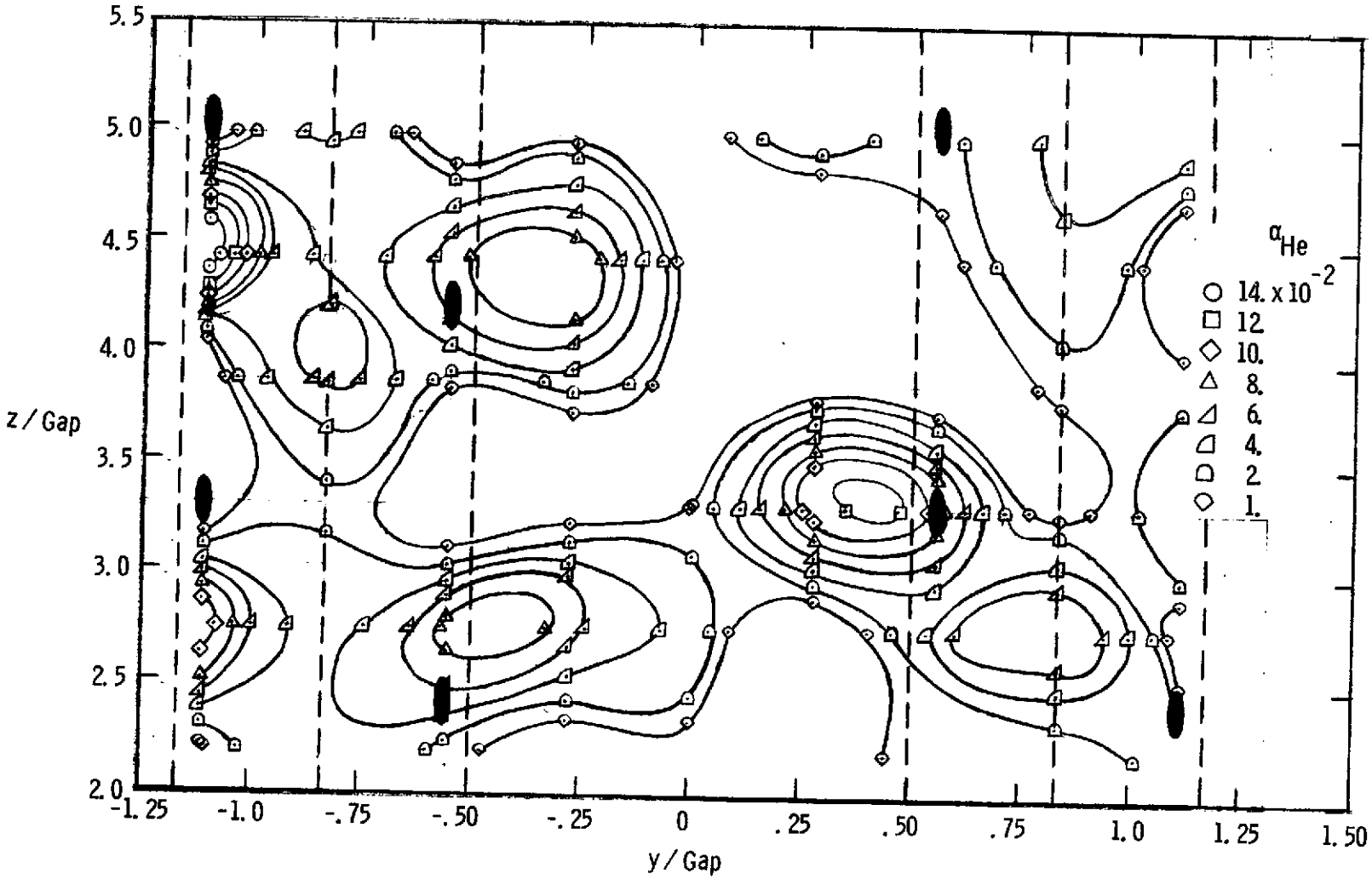

(a) x / Gap = 5.0

Figure 14. - Helium mass concentration contour, Configuration II.

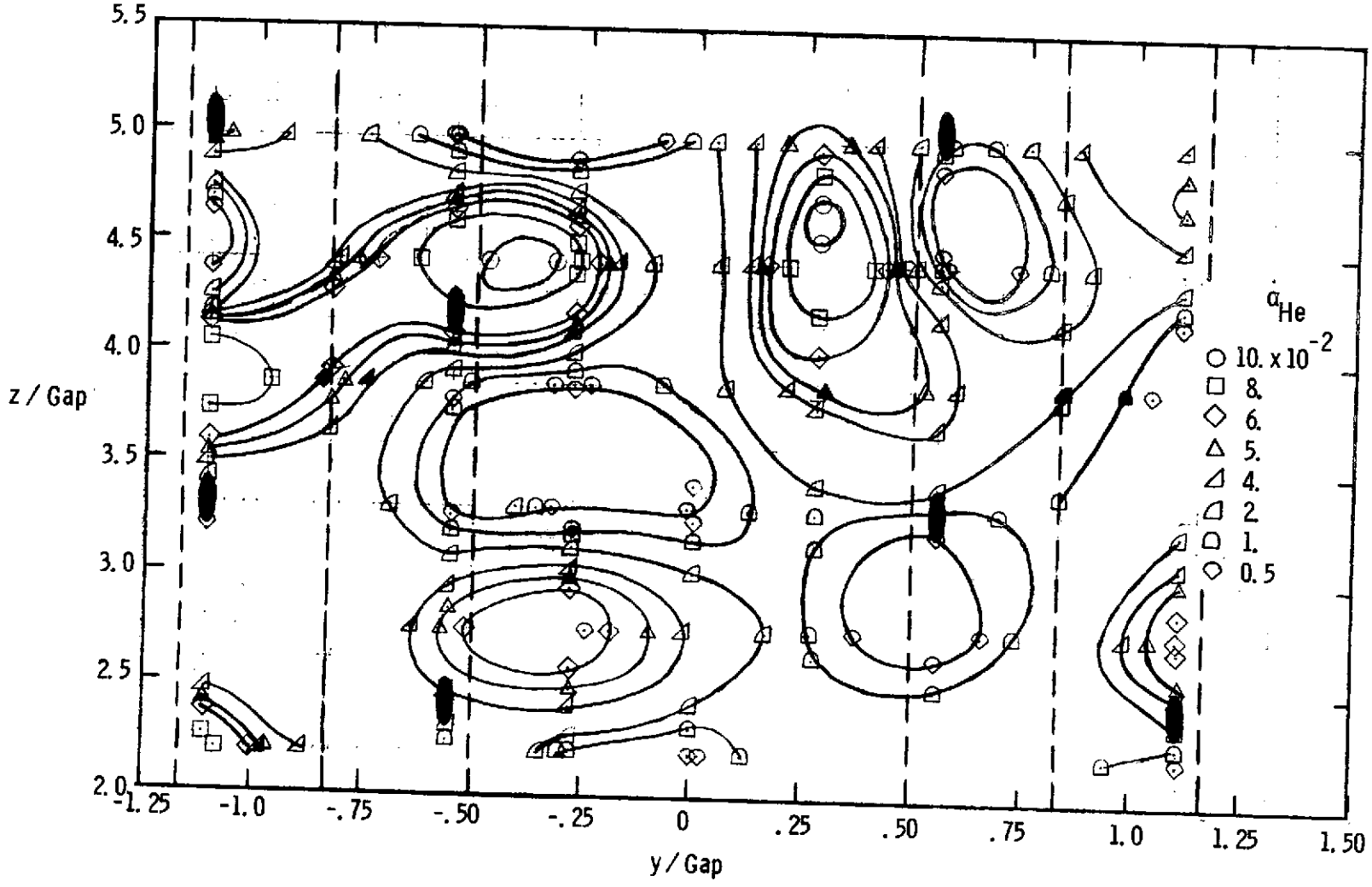

(b) x / Gap = 7.2

Figure 14. - Continued.

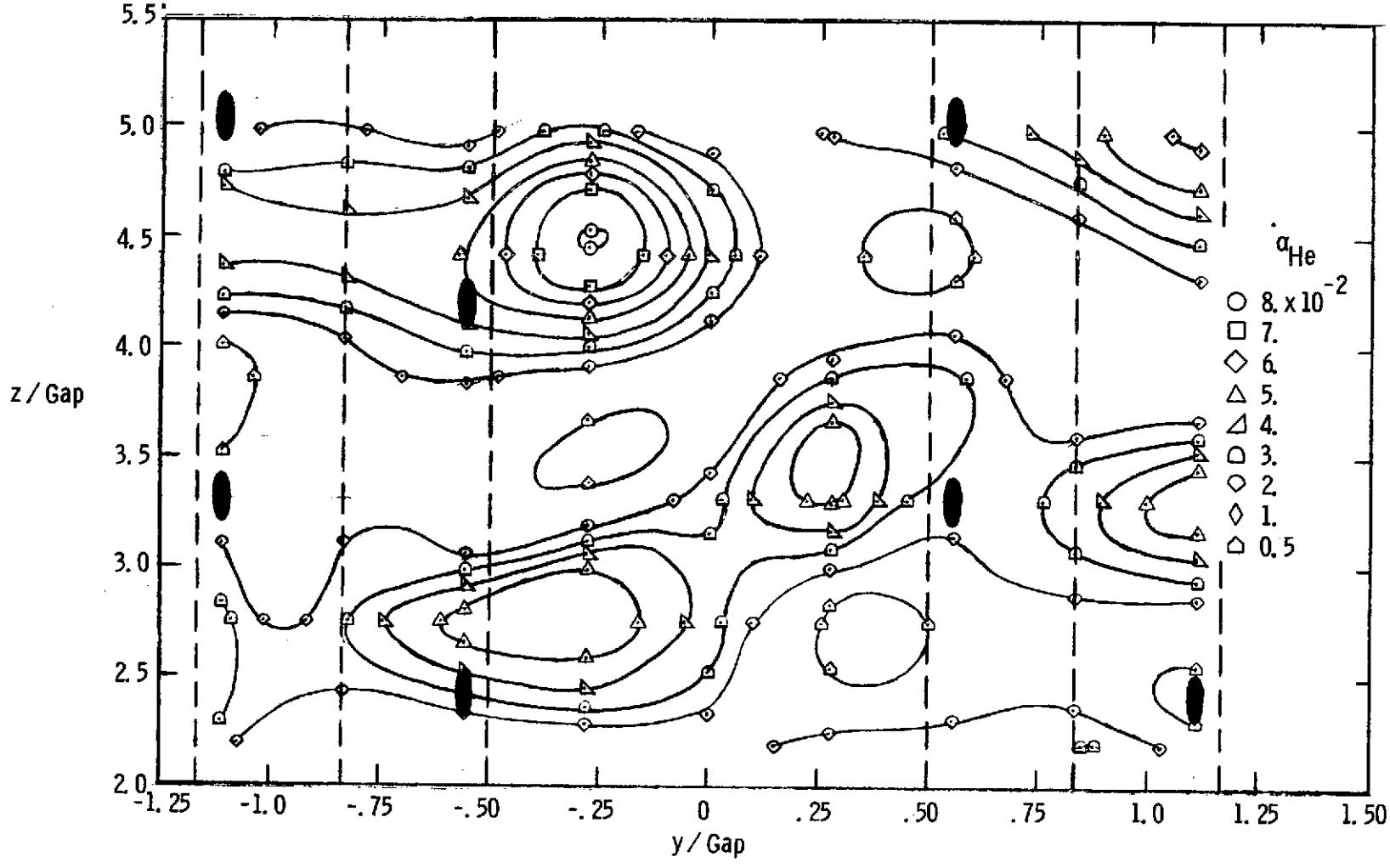

(c) x / Gap = 11.6

Figure 14. - Continued.

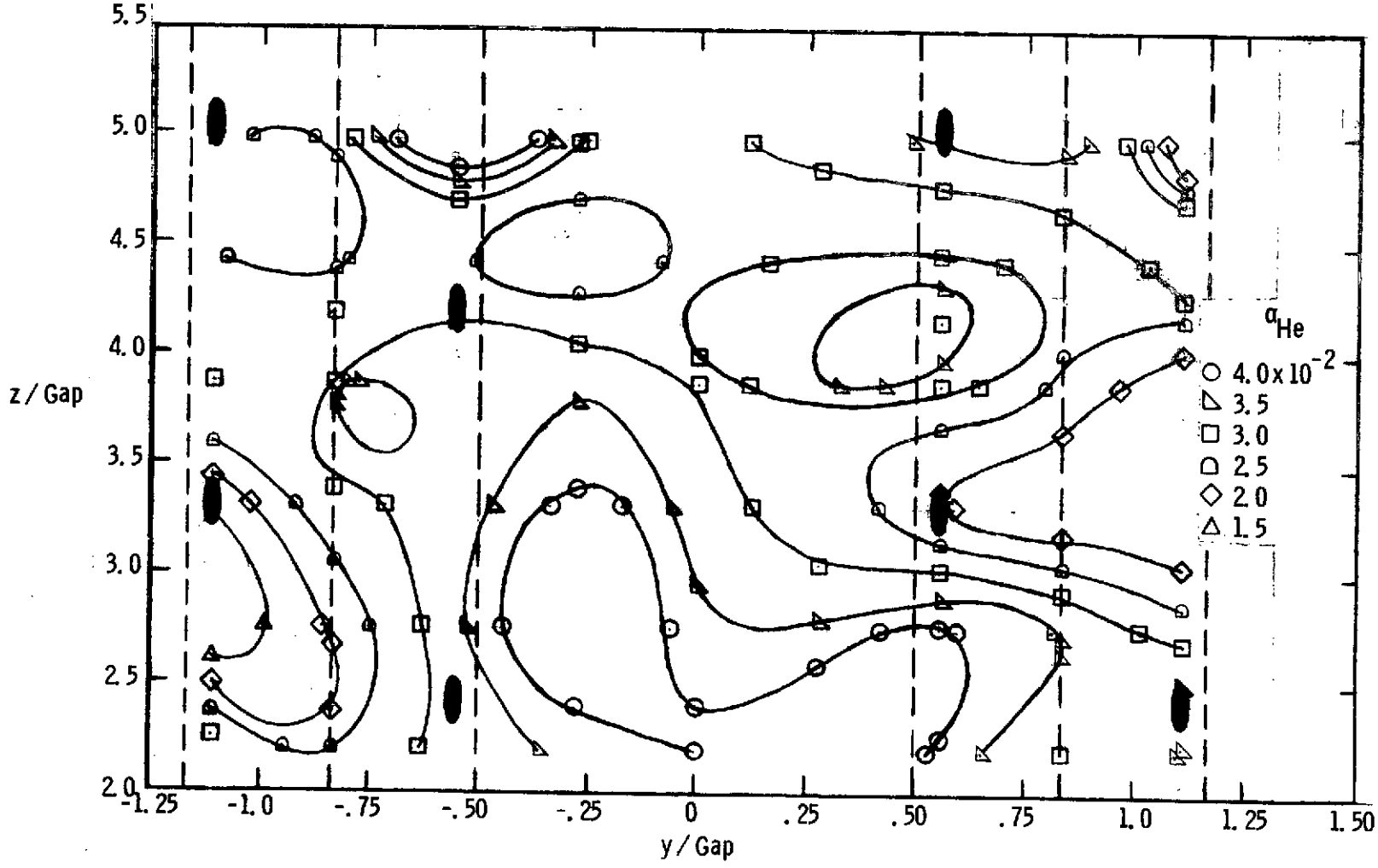

(d) x / Gap = 22.7

Figure 14. - Concluded.

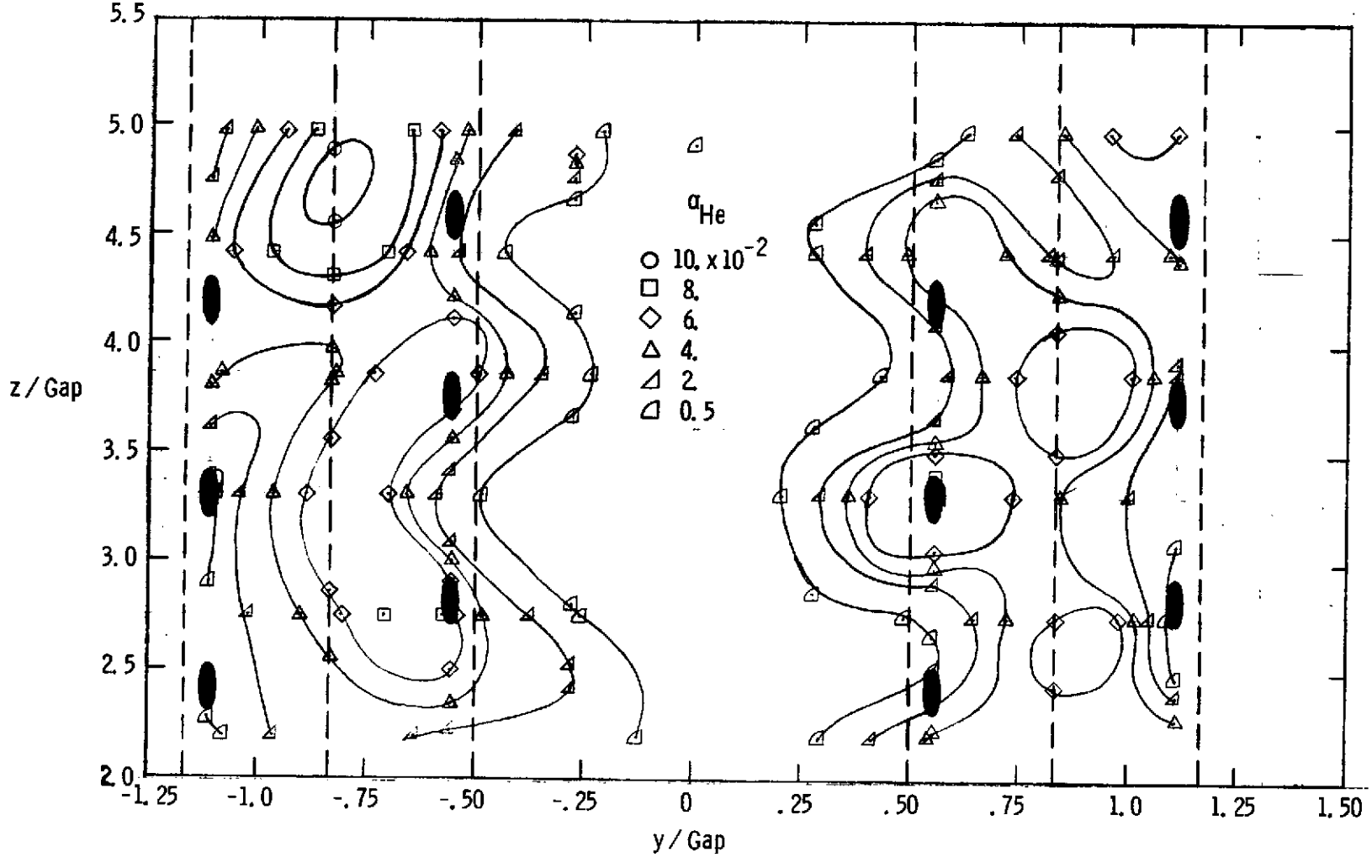

(a) x / Gap = 5.0

Figure 15. - Helium mass concentration contour, Configuration III .

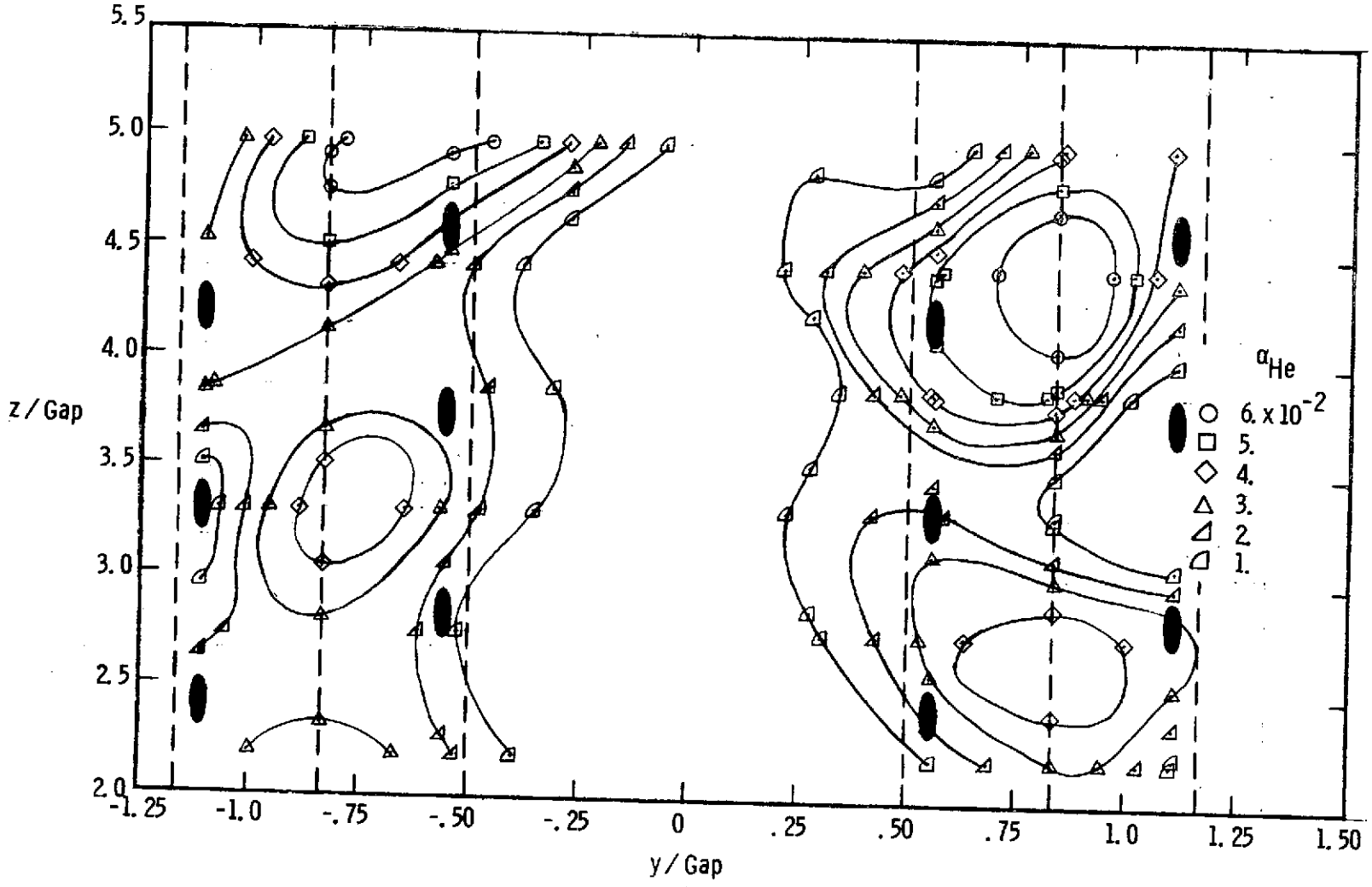

(b) x / Gap = 7.2

Figure 15. - Continued.

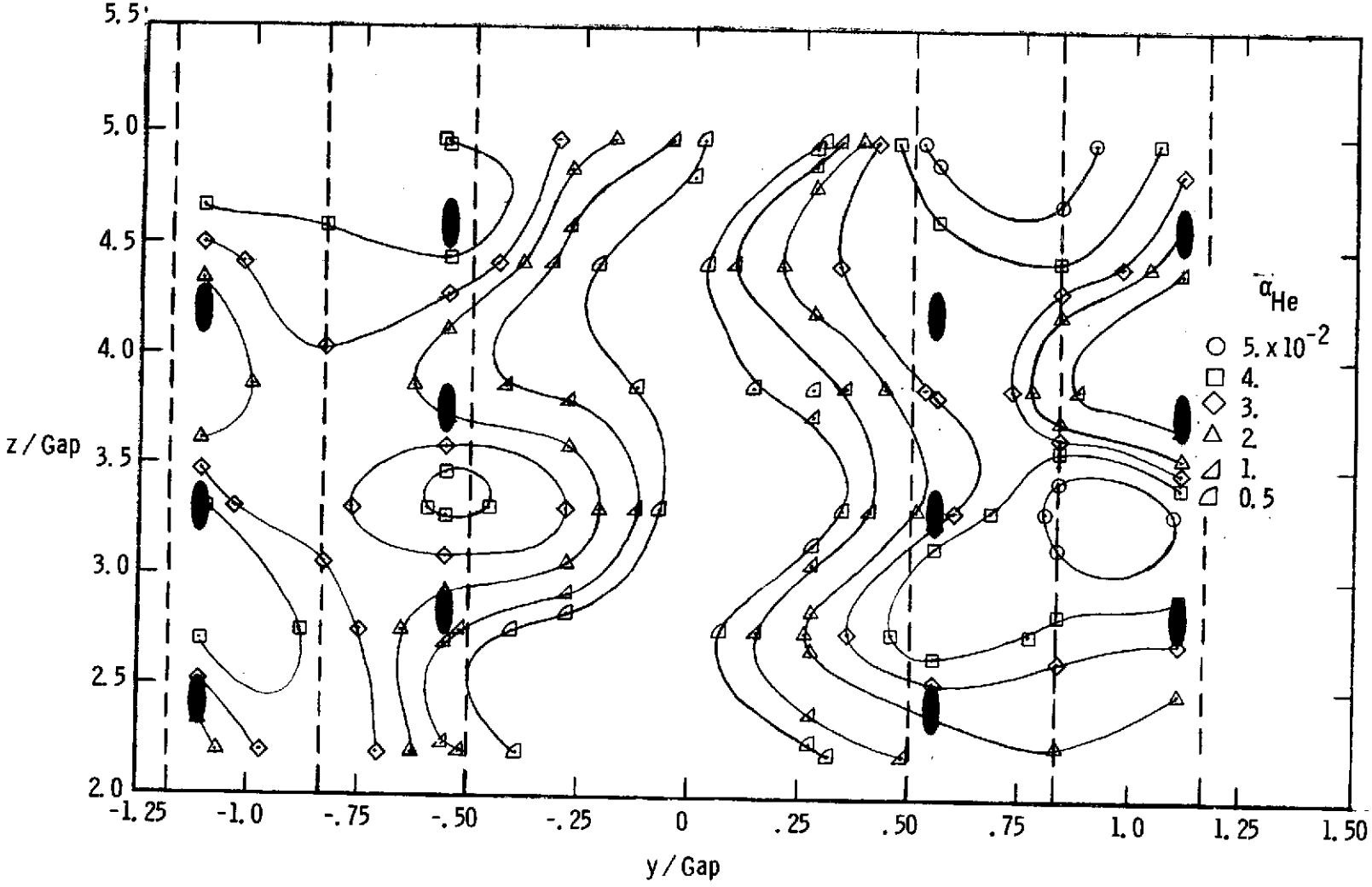

(c) x / Gap = 11.6

Figure 15. - Continued.

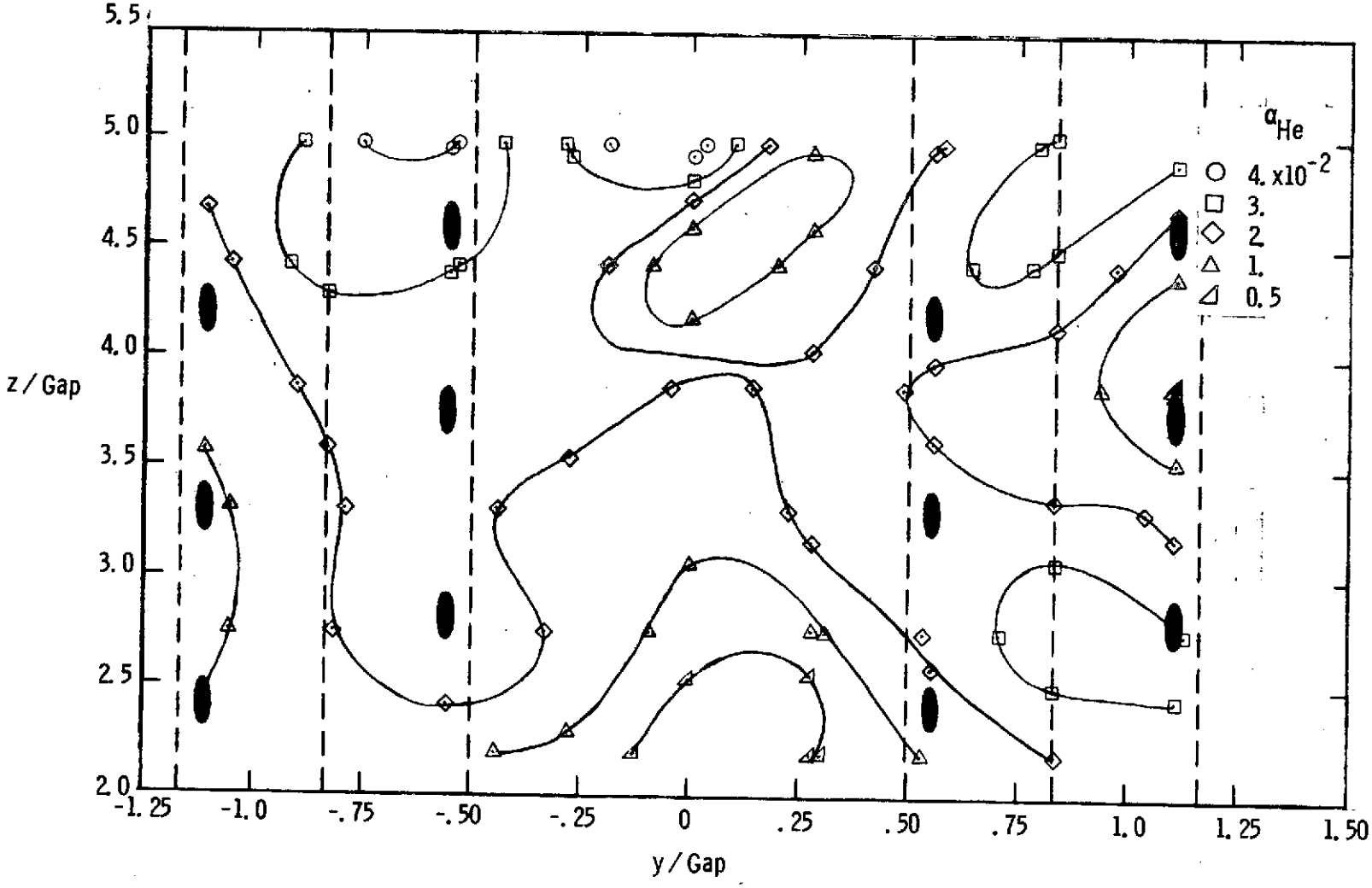

(d) x / Gap = 22.7

Figure 15. - Concluded.

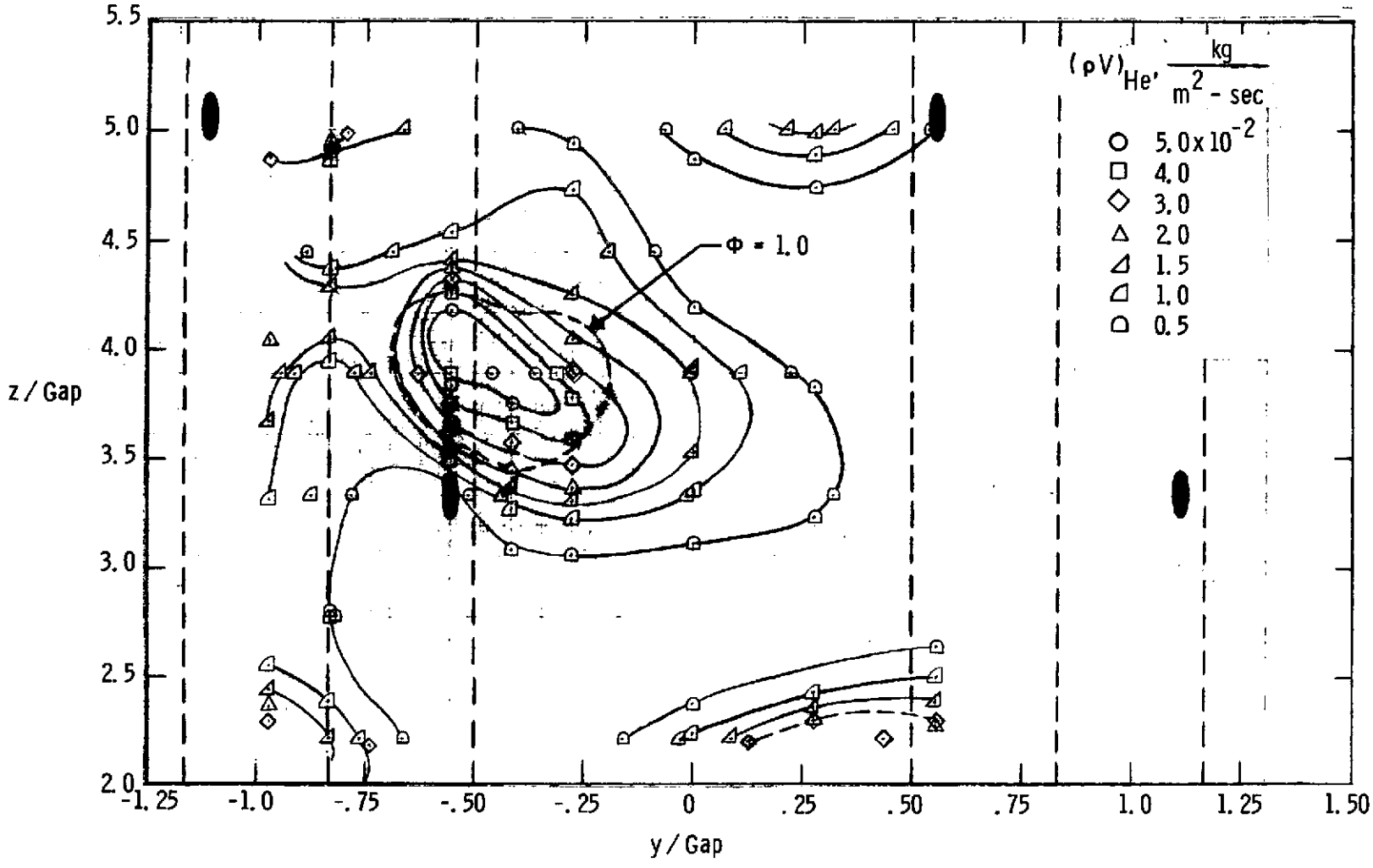

Figure 16. - Sample helium mass flow contour, Configuration I, x/Gap = 11.6

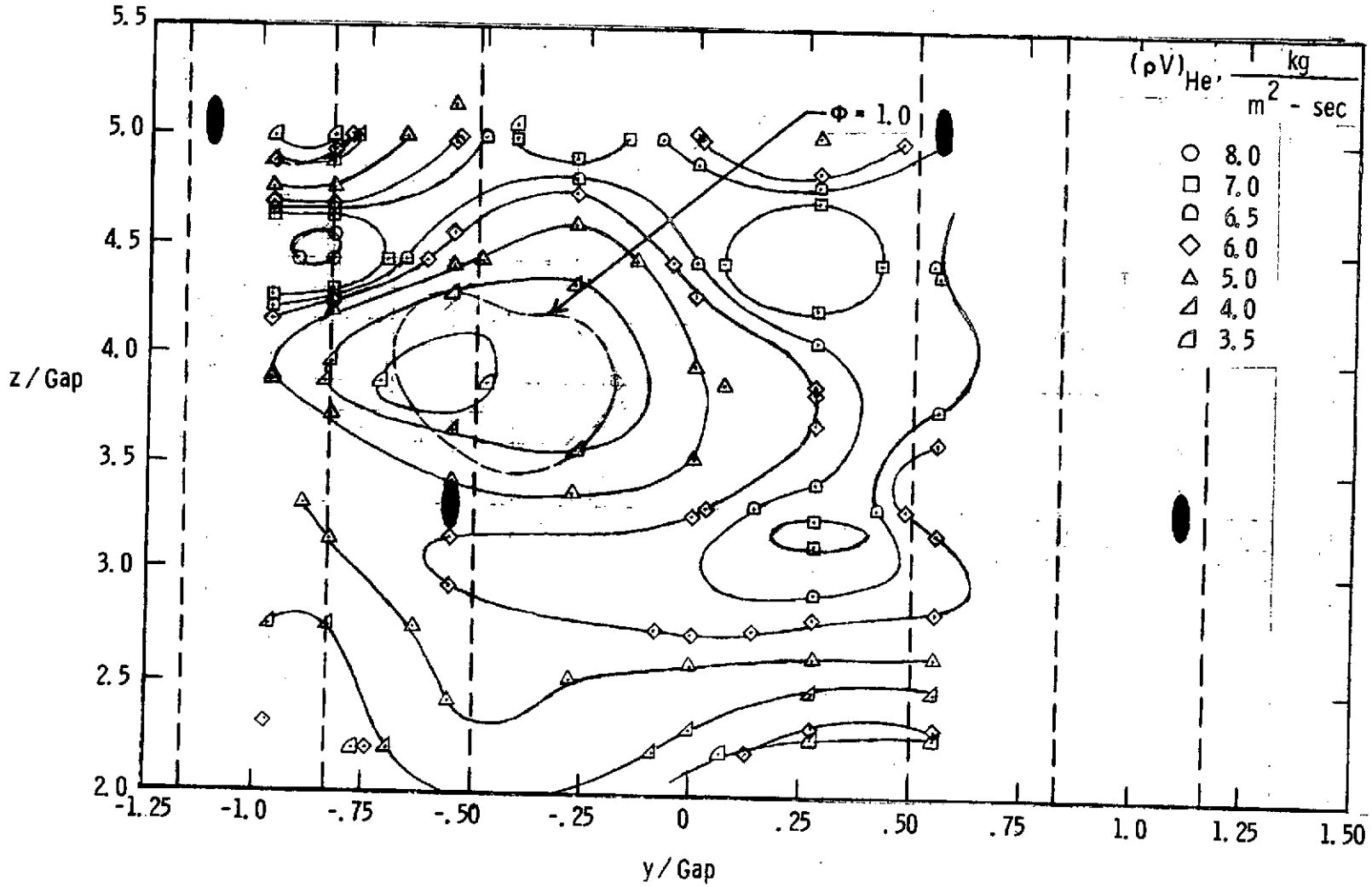

Figure 17. - Sample air mass flow contour, Configuration I, x / Gap = 11.6

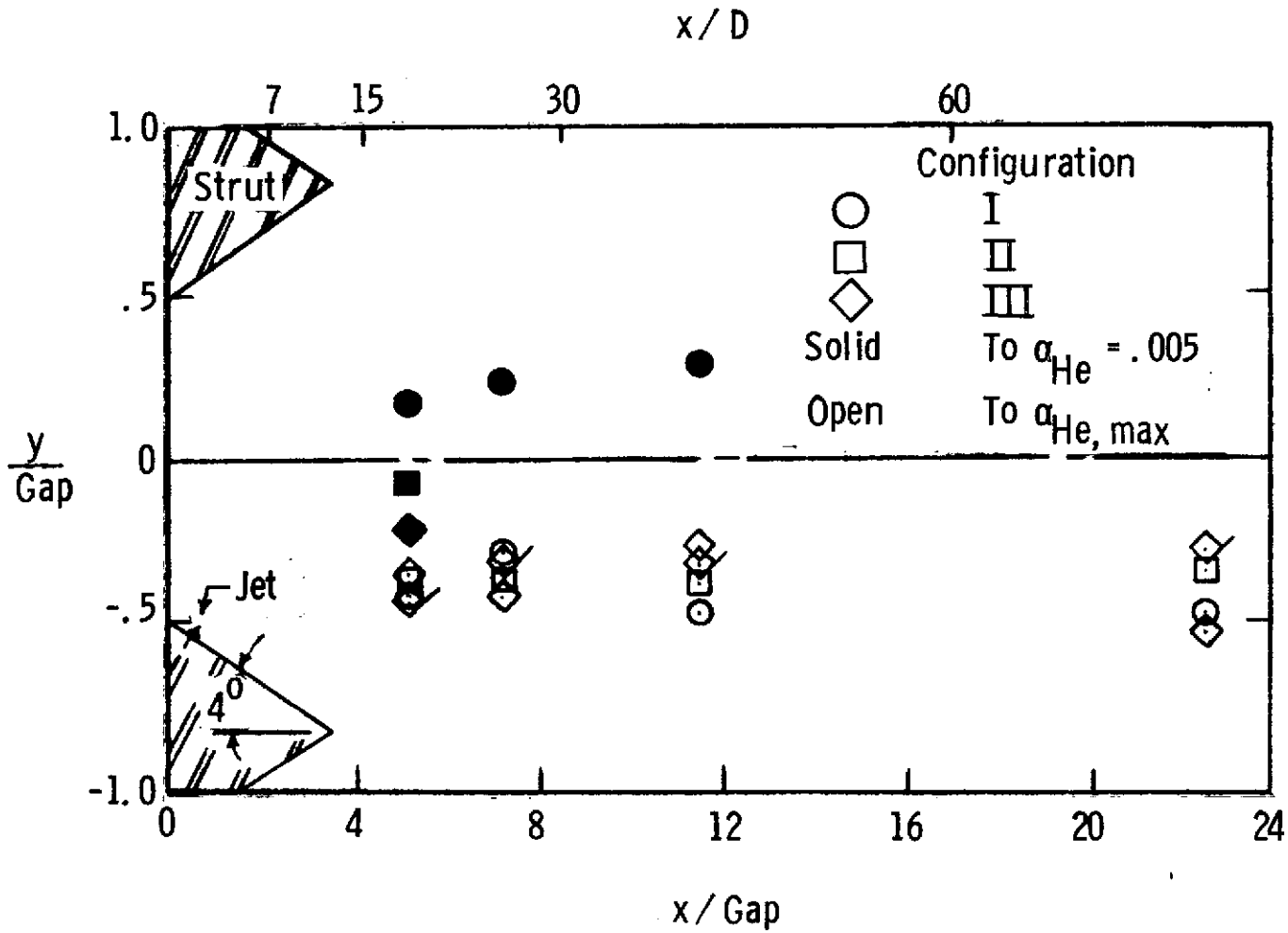

Figure 18. - Helium penetration.

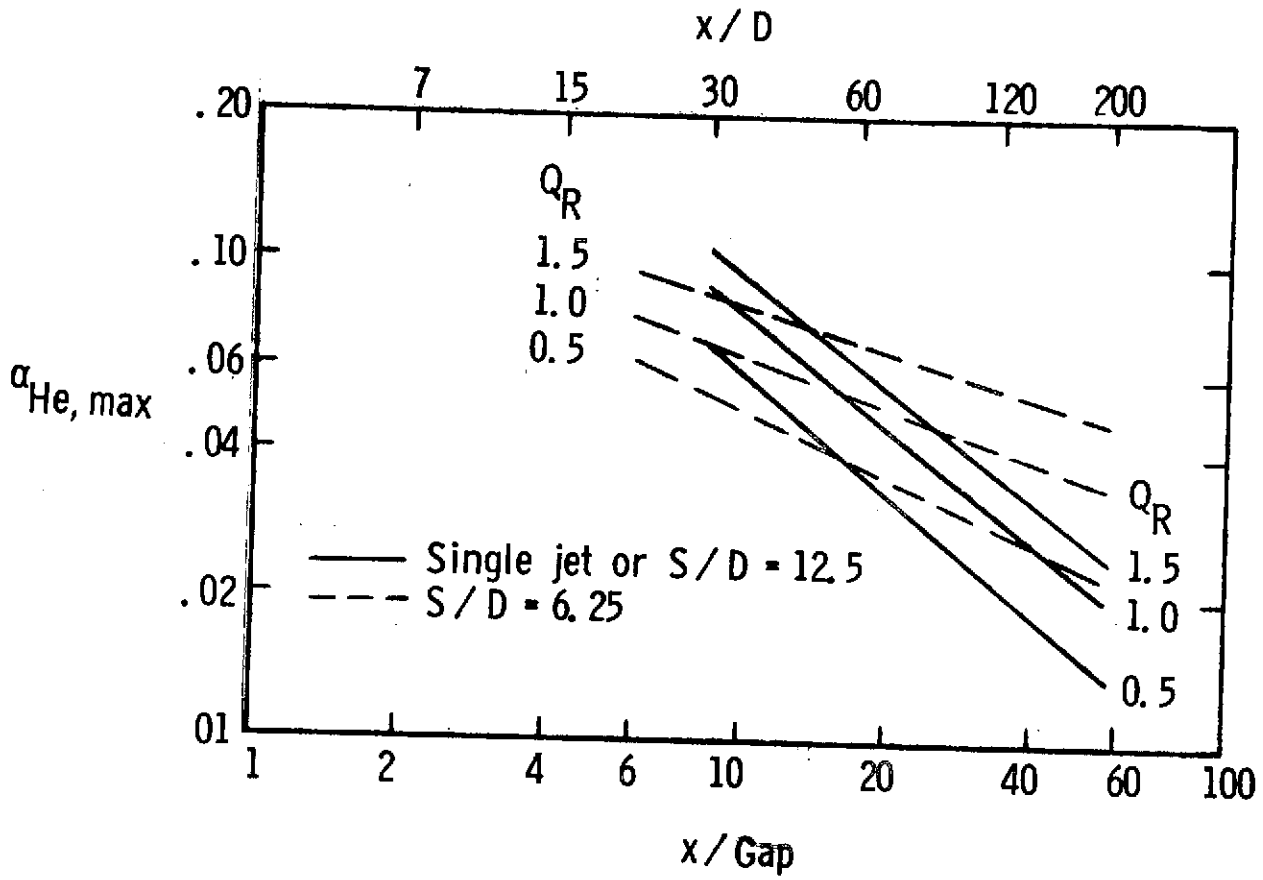

(a) Flat plate results, References 5 and 6.

Figure 19. - Decay of maximum concentration.

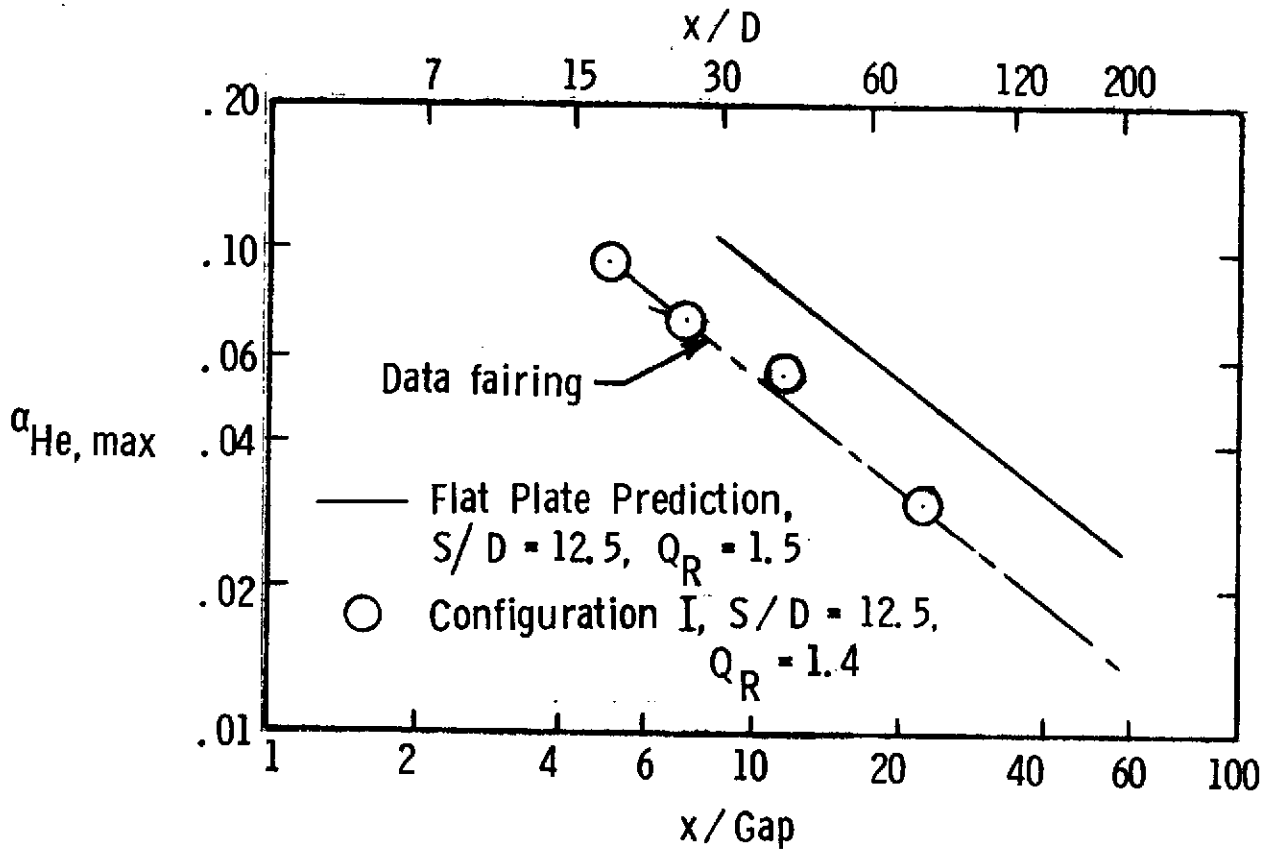

(b) Configuration I comparison with flat plate.

Figure 19. - Continued.

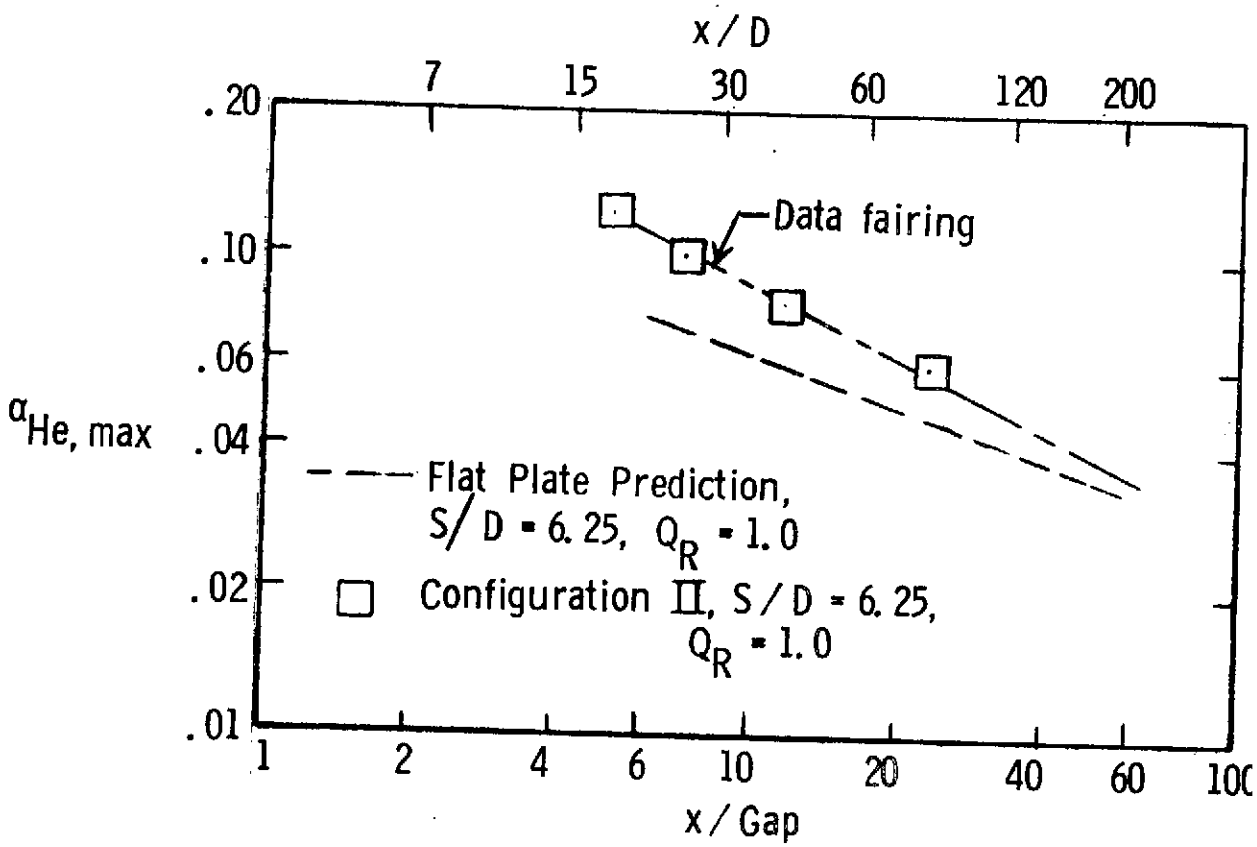

(c) Configuration II comparison with flat plate.

Figure 19. - Continued.

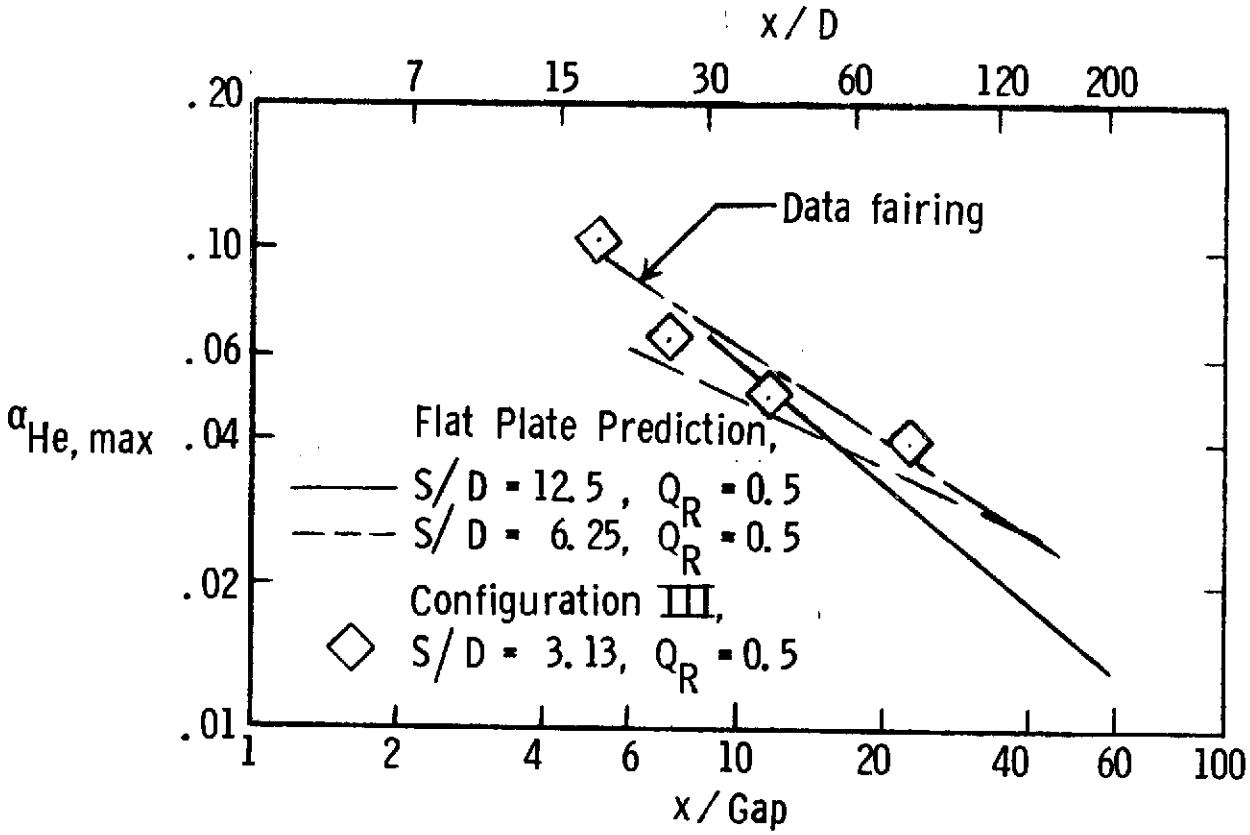

(d) Configuration III comparison with flat plate.

Figure 19. - Concluded.

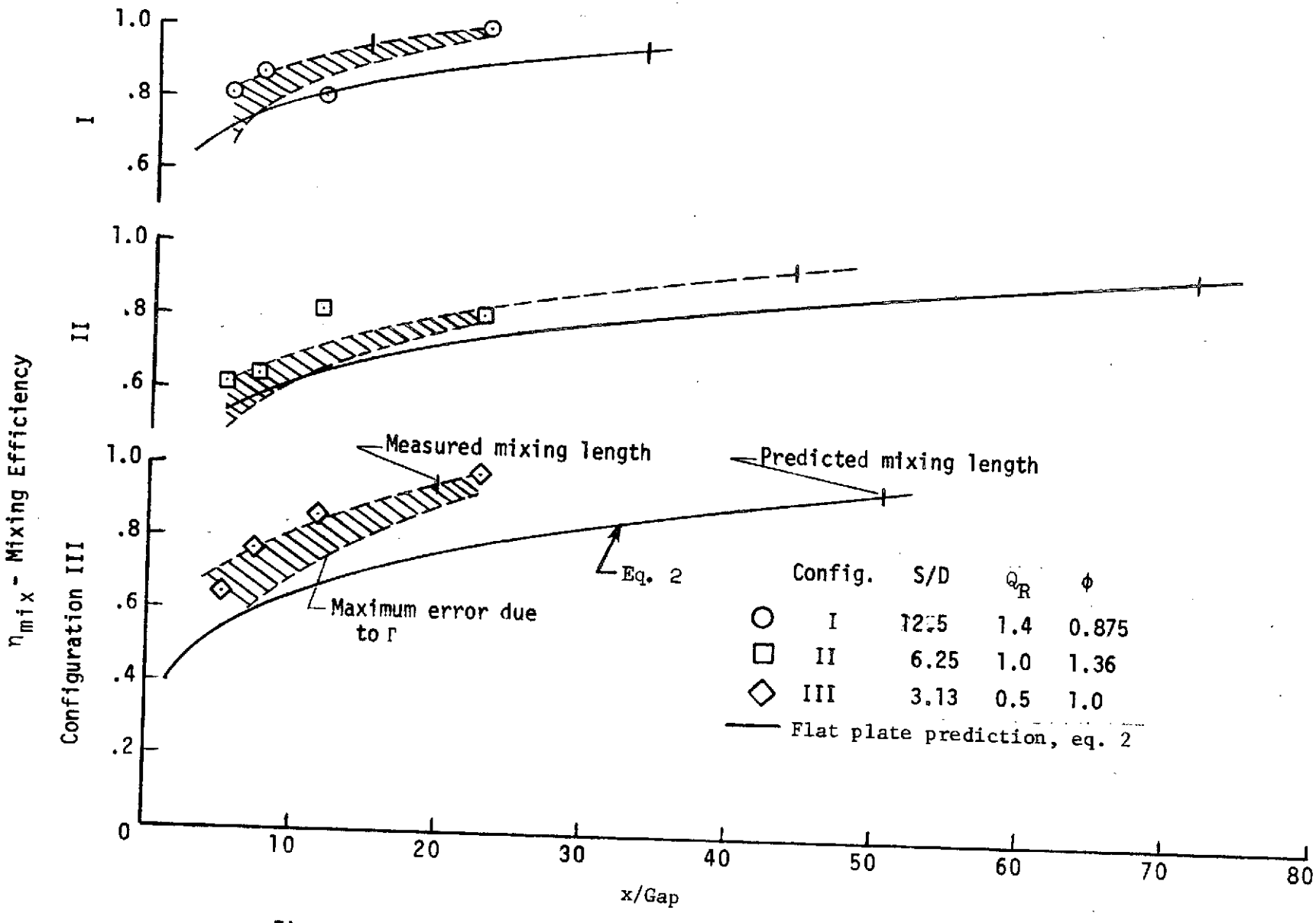

Figure 20.- Measured and Predicted Mixing Lengths.

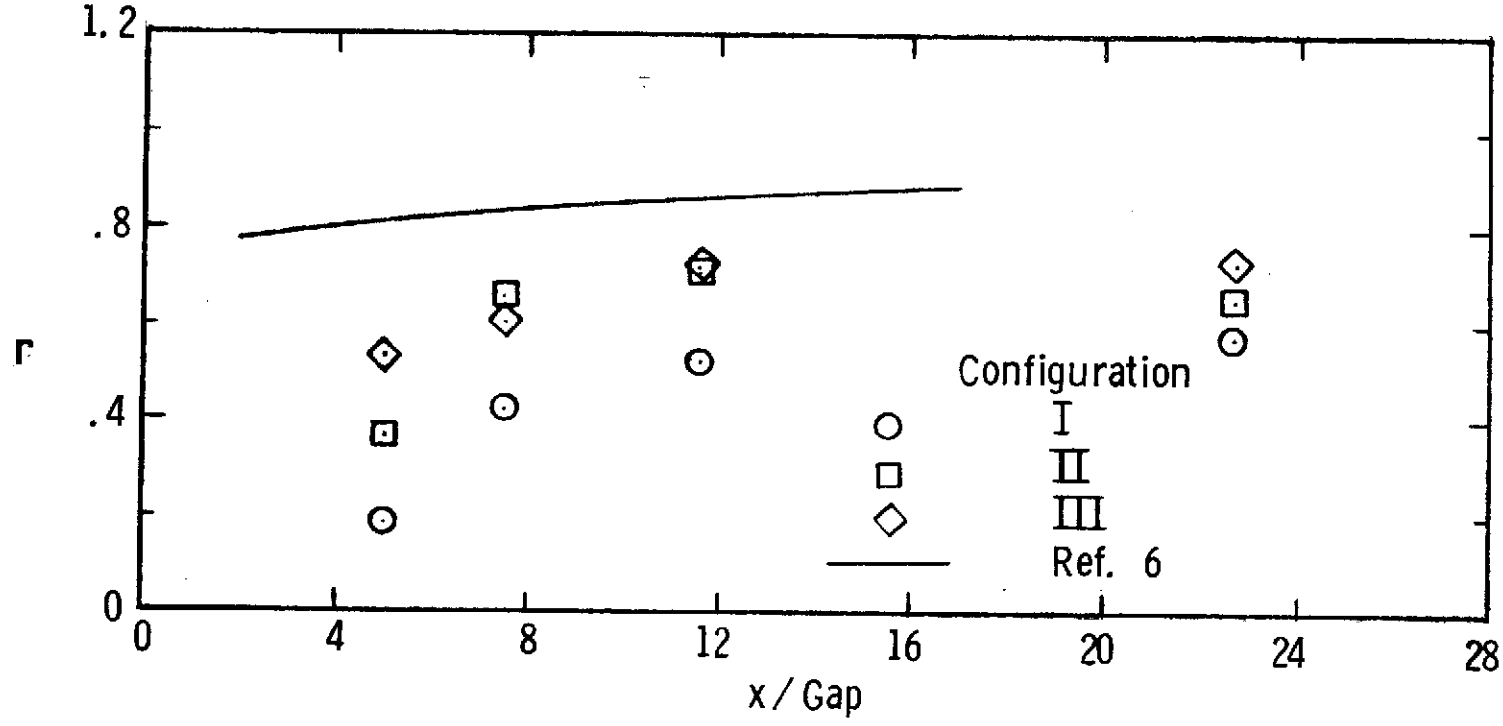

Figure A1. - Ratio of integrated mass flow rate to measured injected mass flow rate.